Inorganic Chemistry

Article

pubs.acs.org/IC

U–CN versus Ce–NC Coordination in Trivalent Complexes Derived from $M[N(SiMe_3)_2]_3$ (M = Ce, U)

Alexandre Hervé,[†] Yamina Bouzidi,[‡] Jean-Claude Berthet,*[,†] Lotfi Belkhiri,[‡] Pierre Thuéry,[†] Abdou Boucekkine,*[,§] and Michel Ephritikhine*[,†]

[†]CEA, IRAMIS, NIMBE, UMR 3299 CEA/CNRS SIS2M, CEA/Saclay, Bat 125, 91191 Gif-sur-Yvette, France

[‡]URCHEMS, Département de Chimie, Université Constantine 1, 25000 Constantine, Algeria

[§]Institut des Sciences Chimiques de Rennes, UMR 6226 CNRS-Université de Rennes 1, Campus de Beaulieu, 35042 Rennes Cedex, France

Supporting Information

ABSTRACT: Reactions of $[MN^*_3]$ (M = Ce, U; N* = $N(SiMe_3)_2$) and NR_4CN (R = Me, Et, or ^{n}Bu) or KCN in the presence of 18-crown-6 afforded the series of cyanido-bridged dinuclear compounds $[NEt_4][(MN^*_3)_2(\mu\text{-CN})]$ (M = Ce, **2a**, and U, **2b**), $[K(18\text{-crown-6})(THF)_2][(CeN^*_3)_2(\mu\text{-CN})]$ (**2′a**), and $[K(18\text{-crown-6})][(UN^*_3)_2(\mu\text{-CN})]$ (**2′b**), and the mononuclear mono-, bis-, and tris(cyanide) complexes $[NEt_4][MN^*_3(CN)]$ (M = Ce, $\mathbf{1a^{Et}}$, and U, $\mathbf{1b^{Et}}$), $[NMe_4][MN^*_3(CN)]$ (M = Ce, $\mathbf{1a^{Me}}$, and U, $\mathbf{1b^{Me}}$), $[K(18\text{-crown-6})][MN^*_3(CN)]$ (M = Ce, **1′a**, and U, **1′b**), $[N^nBu_4]_2[MN^*_3(CN)_2]$ (M = Ce, **3a**, and U, **3b**), $[K(18\text{-crown-6})]_2[MN^*_3(CN)_2]$ (M = Ce, **3′a**, and U, **3′b**), and $[N^nBu_4]_2[MN^*_2(CN)_3]$ (M = Ce, **4a**, and U, **4b**). The mono- and bis(cyanide) complexes were found to be in equilibrium. The formation constant of **3′b** ($K_{3'b}$) from **1′b** at 10 °C in THF is equal to $5(1) \times 10^{-3}$, and $-\Delta H_{3'b}$ = 104(2) kJ mol^{-1} and $-\Delta S_{3'b}$ = 330(5) J mol^{-1} K^{-1}. The bis(cyanide) compound **3a** or **3b** was slowly transformed in solution into an equimolar mixture of the mono- and tris(cyanide) derivatives with elimination of $N^nBu_4N^*$. The crystal structures of $\mathbf{1a^{Me}}$, $\mathbf{1b^{Me}}$, **1′a**·toluene, **1′b**·toluene, **2′a**, **2′b**, **3a**, **3′a**, **3′b**, **3′a**·2benzene, **3′b**·2benzene, **4a**·0.5THF, and **4b**·Et_2O were determined. Crystals of the bis(cyanide) uranium complexes **3′b** and **3′b**·2benzene are isomorphous with those of the cerium counterparts **3′a** and **3′a**·2benzene, but they are not isostructural since the data revealed distinct coordination modes of the CN group, through the C or N atom to the U or Ce metal center, respectively. This differentiation has been analyzed using density functional theory calculations. The observed preferential coordination of the cyanide and isocyanide ions toward uranium or cerium in the bis(cyanide) complexes is corroborated by the consideration of the binding energies of these groups to the metals and by the comparison of DFT optimized geometries with the crystal structures. The better affinity of the cyanide ligand toward U^{III} over Ce^{III} metal center is related to the better energy matching between the 6d/5f uranium orbitals and the cyanide ligand ones, leading to a non-negligible covalent character of the bonding.

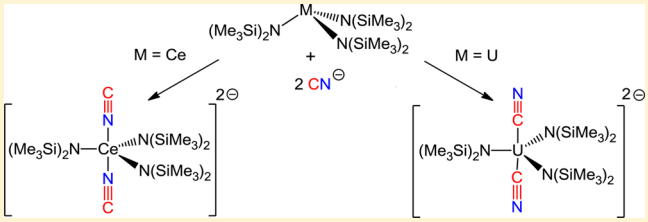

INTRODUCTION

The first cyanide compounds of the f elements were synthesized in the early 1970s. Reactions in anhydrous liquid ammonia of a lanthanide metal (Ln) with NH_4CN and of UCl_4 with an alkali metal cyanide gave $[Ln(CN)_x]$ (x = 3 and Ln = Ce, Pr, Ho, Sm, Eu, Yb, or x = 2 and Ln = Sm, Eu, Yb)[1] and $[UCl_3(CN)\cdot 4NH_3]$,[2] respectively. The organometallic complexes $[M(Cp)_2(CN)]$ (M = Nd, Yb, U; Cp = η-C_5H_5) and $[U(Cp)_3(CN)]$ were obtained by protonolysis of $[M(Cp)_3]$ and $[U(Cp)_4]$ with HCN in benzene,[3] while the tris(cyclopentadienyl) and bis(indenyl) cerium(IV) cyanides $[Ce(Cp)_3(CN)]$ and $[Ce(C_9H_7)_2(CN)_2]$ were synthesized by treatment of the corresponding chlorides with KCN.[4] The tris(cyclopentadienyl) derivatives $[U(C_5H_4R)_3(CN)]$ were subsequently isolated from salt metathesis reactions of $[U(C_5H_4R)_3Cl]$ (R = H, Me) with alkali metal cyanides,[5] oxidation of $[U(C_5H_4R)_3]$ (R = H, ^{t}Bu) with nitrile[6] or isonitrile molecules,[7,8] and addition of N^nBu_4CN to the cationic precursor $[U(C_5H_4SiMe_3)_3][BPh_4]$.[7,8] In view of their very poor solubility in usual organic solvents, most of these complexes were supposed to have a polymeric structure ensured by strong CN bridges. Indeed, the first structurally characterized complexes were the cyclic trimeric and hexameric samarium compounds $[Sm(Cp^*)_2(\mu\text{-CN})(CNC_6H_{11})]_3$[9] and $[Sm(Cp^*)_2(\mu\text{-CN})]_6$ (Cp* = η-C_5Me_5).[10] The former was synthesized by reaction of $[Sm(Cp^*)_2(THF)_2]$ with cyclohexyl isocyanide,[9] while the latter was isolated from a mixture of $[Sm(Cp^*)_2(CH\{SiMe_3\}_2)]$ and *N*-benzylidene(trimethylsilyl)-amine under H_2 pressure.[10] A series of analogous trinuclear complexes $[M(Cp^*)_2(\mu\text{-CN})(L)]_3$ were subsequently synthesized (M = La or Pr and L = Me_3SiCN;[11,12] M = Ce, Sm, or U

Received: April 23, 2014
Published: June 16, 2014

   dx.doi.org/10.1021/ic500939t | *Inorg. Chem.* 2014, 53, 6995–7013

Scheme 1. Synthesis of the Complexes

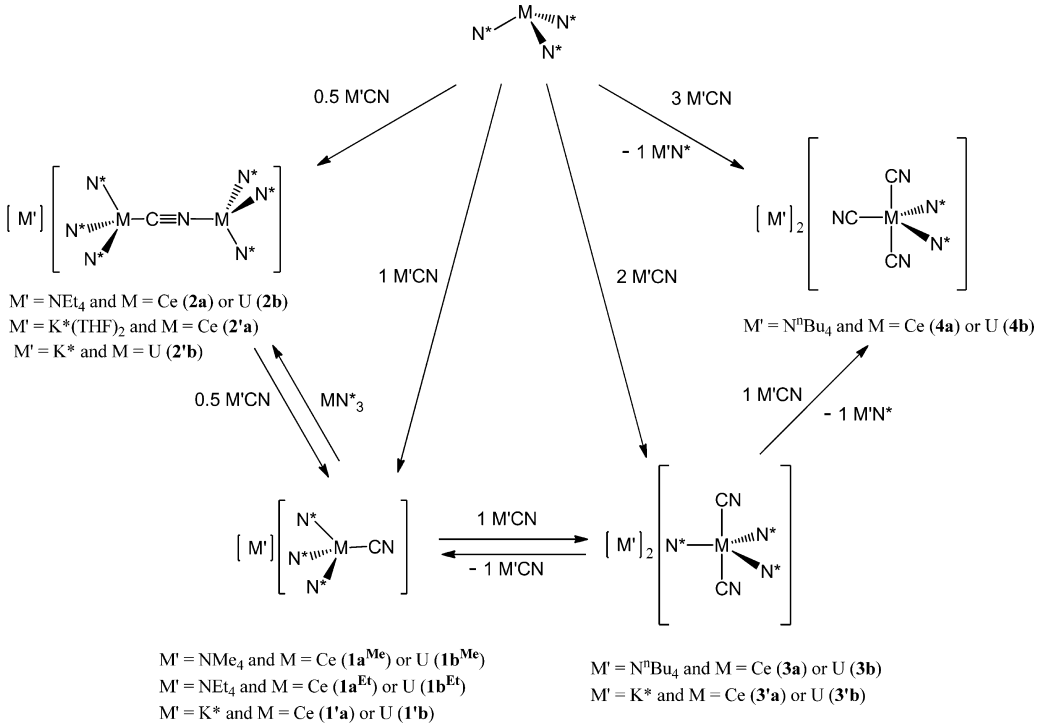

and L = ^{t}BuNC;[12,13] M = Sm and L = ^{t}BuCN[14]) by oxidation of $[Sm(Cp^*)_2(THF)_2]$ with ^{t}BuCN,[14] salt metathesis reaction of $[Ce(Cp^*)_2I]$ with N^nBu_4CN in the presence of ^{t}BuNC,[13] and sterically induced reductions of $[M(Cp^*)_3]$ (M = La, Pr, Sm, U)[11,12] in the presence of Me_3SiCN, ^{t}BuNC, or ^{t}BuCN. The ability of the CN group to link various metal ions led to a wide diversity of heteropolynuclear assemblies which contain d transition metals and lanthanides and attract much attention for their magnetic properties.[15]

After the tris(cyclopentadienyl) complex $[U(C_5Me_4H)_3(CN)_{0.4}(Cl)_{0.6}]$,[16] which was serendipitously obtained from the decomposition of the alkyl isocyanide derivative $[U(C_5Me_4H)_3(CN^tBu)]$ and for which the coordination mode of the CN ligand could not be specified due to the disorder present in the crystal, the first mononuclear cyanide compound to have been crystallographically characterized was the bis(cyclopentadienyl) complex $[U(C_5{}^tBu_3H_2)_2(CN)(OSiMe_3)]$ resulting from the reaction of the oxo precursor $[U(C_5{}^tBu_3H_2)_2(=O)]$ with Me_3SiCN.[17] It was found later that the same reaction of the thorium counterpart gave the isocyanide derivative $[Th(C_5{}^tBu_3H_2)_2(NC)(OSiMe_3)]$, a difference which has not been mentioned.[18]

The very limited number of uranium cyanide complexes incited us to develop this class of compounds, and the use of the CN ligand led to the discovery of unprecedented structures. Treatment of $[U(Cp^*)_2X_2]$ (X = I, OSO_2CF_3) with NR_4CN (R = Et, ^{n}Bu) gave successively the bis- and tris(cyanide) derivatives $[U(Cp^*)_2(CN)_2]$, $[NR_4][U(Cp^*)_2(CN)_3]$ and the novel type of linear metallocene $[NR_4]_3[U(Cp^*)_2(CN)_5]$ in which the equatorial plane is completely filled with five CN ligands.[8,19] The cyanide group was found to be an efficient wedge for bending the very stable actinocene $[An(Cot)_2]$ into $[An(Cot)_2(CN)]^-$ (COT = η^8-C_8H_8, An = U,[20] Th[21]), the first bent bis(cyclooctatetraenyl) compounds. The anionic cyanide complexes of (*N*,*C*), (*N*,*N*), and (*N*,*O*) metallacycles of tetra- and pentavalent uranium $M[UN^*_2(N,C)(CN)]$, $[NEt_4][UN^*(N,O)_2(CN)_2]$, and $M[UN^*(N,O)_2(CN)]$ were synthesized by addition of MCN [M = Na(15-crown-5) or NEt_4] to $[UN^*_2(N,C)]$ [N* = $N(SiMe_3)_2$; *N*,*C* = $CH_2SiMe_2N(SiMe_3)$], $[UN^*(N,N)I]$ [*N*,*N* = $(Me_3Si)NSiMe_2CH_2CH_2SiMe_2N(SiMe_3)$], and $[Na\{UN^*(N,O)_2\}_2(\mu\text{-}I)]$ [*N*,*O* = $OC(=CH_2)SiMe_2N(SiMe_3)$], respectively.[22] Although the cyanide ligand was claimed to be anathema to uranium(VI) because the carbon end of CN was considered as a strong σ donor and a good π acceptor[23] (the preference for C or N atom coordination being however controversial[24,25]), the uranyl cyanide $[NEt_4]_3[UO_2(CN)_5]$ was readily prepared by treating $[UO_2(OSO_2CF_3)_2]$ with NEt_4CN,[26] and $[NEt_4]_2[UO_2(Cp^*)(CN)_3]$, the first cyclopentadienyl complex of uranyl, was isolated from reaction of $[NEt_4]_3[U(Cp^*)_2(CN)_5]$ and pyridine *N*-oxide.[27]

By comparison with the large number of cyanide complexes of the main group and d transition metals, such compounds of the f elements are much less numerous, and in particular, mononuclear cyanide complexes of trivalent lanthanides and actinides are quite rare, while these species would be valuable building blocks for the synthesis of novel clusters and coordination polymers with interesting physicochemical properties. The bis(cyclopentadienyl) compounds $[N^nBu_4]_2[M(Cp^*)_2(CN)_3]$ (M = Ce, U), obtained by addition of N^nBu_4CN to $[M(Cp^*)_2X]$ (X = I, OSO_2CF_3), are the only ones to have been crystallographically characterized, and the high accuracy of the structures permitted the unambiguous determination of the M−C bonding mode of the CN ion.[13] Here we report on the series of analogous cerium(III) and uranium(III) cyanide compounds $[M'][(MN^*_3)_2(\mu\text{-}CN)]$, $[M'][MN^*_3(CN)]$, $[M']_2[MN^*_3(CN)_2]$, and $[M']_2[MN^*_2(CN)_3]$ [M′ = K(18-crown-6), NMe_4, NEt_4, or N^nBu_4; M = Ce or U) which have been synthesized by successive additions of M′CN to $[MN^*_3]$. The dynamic behavior of the complexes in solution is described. The X-ray crystal structures of all the complexes are presented with special attention to those of the

dx.doi.org/10.1021/ic500939t | Inorg. Chem. 2014, 53, 6995−7013

bis(cyanide) derivatives $[M']_2[MN^*_3(CN)_2]$ which exhibit distinct coordination modes of the CN group, through the C or N atom to the U or Ce metal center, respectively. This differentiation has been analyzed using relativistic density functional theory (DFT) calculations.

RESULTS AND DISCUSSION

The syntheses of the complexes are summarized in Scheme 1, without giving true description of the CN bonding mode (through C or N atom) and of the interaction of K(18-crown-6) with the CN groups, which will be discussed hereafter. For isostructural compounds, suffixes **a** and **b** correspond to cerium and uranium analogues ($[N^nBu_4]_2[CeN^*_3(CN)_2]$ (**3a**) and $[N^nBu_4]_2[UN^*_3(CN)_2]$ (**3b**) for example), while un-primed and primed complexes denote ammonium and potassium salts, respectively ($[N^nBu_4]_2[CeN^*_3(CN)_2]$ (**3a**) and $[K(18\text{-crown-}6)]_2[MN^*_3(CN)_2]$ (**3′a**) for example). In the only case of the monocyanide derivatives $[NR_4][MN^*_3(CN)]$ (M = Ce, U), two ammonium salts have been used with R = Me and Et, leading to the formation of two pairs of complexes $\mathbf{1a}^{Me}$ and $\mathbf{1b}^{Me}$, $\mathbf{1a}^{Et}$ and $\mathbf{1b}^{Et}$.

Mono(cyanide) and Cyanido-Bridged Complexes $[M'][MN^*_3(CN)]$ and $[M'][(MN^*_3)_2(\mu\text{-CN})]$. First experiments were focused on the equimolar mixtures of M′CN and $[MN^*_3]$. In the presence of 1 mol equiv of NEt_4CN in toluene or THF, $[CeN^*_3]$ and $[UN^*_3]$ were readily transformed into the anionic complexes $[NEt_4][CeN^*_3(CN)]$ ($\mathbf{1a}^{Et}$) and $[NEt_4][UN^*_3(CN)]$ ($\mathbf{1b}^{Et}$) which were isolated in 99% and 78% yields as yellowish and dark blue powders, respectively. The ^{1}H NMR spectrum in THF-d_8 of $\mathbf{1b}^{Et}$ exhibits at 20 °C a signal at δ_H −5.71 which integrates for 54 H and corresponds to the six $SiMe_3$ groups; decoalescence of this signal is observed at −60 °C, and two singlets of equal intensities at δ_H −25.9 and 4.9 are visible at −90 °C. These features can be explained by the restricted rotation along the U−N bonds, giving two sets of three $SiMe_3$ groups, one pointing toward (*endo*) and the other pointing away (*exo*) from the CN ligand.[28] These two series of $SiMe_3$ groups also give rise to two signals in the ^{13}C NMR spectrum of $\mathbf{1b}^{Et}$, at δ_C −109.0 and −111.0 in benzene-d_6 at 20 °C. Decoalescence of the ^{1}H NMR $SiMe_3$ signal of the cerium analogue $\mathbf{1a}^{Et}$ (δ_H −0.66 at 20 °C) was observed at −85 °C, but the slow-limit spectrum could not be attained.

Crystals of $\mathbf{1a}^{Et}$ and $\mathbf{1b}^{Et}$ suitable for X-ray diffraction could not been obtained and replacement of the ammonium ion NEt_4^+ with an alkali metal ion was then considered. Slow diffusion of pentane into a 1:1:1 mixture of $[CeN^*_3]$, KCN, and 18-crown-6 in THF did not afford crystals of $[K(18\text{-crown-}6)][CeN^*_3(CN)]$ (**1′a**) but yellow crystals of the cyanido-bridged complex $[K(18\text{-crown-}6)(THF)_2][(CeN^*_3)_2(\mu\text{-CN})]$ (**2′a**). The ^{1}H NMR spectra revealed that, in the presence of 5 mol equiv of KCN in THF-d_8, $[CeN^*_3]$ was transformed successively into $[K(THF)_x][(CeN^*_3)_2(\mu\text{-CN})]$ and $[K(THF)_x][CeN^*_3(CN)]$, characterized by their $SiMe_3$ signal at δ_H −2.60 and −0.74, respectively. The rapid formation of the dinuclear compound can be explained by the poor solubility of KCN in organic solvents. The formation of crystals of either the mononuclear mono(cyanide) or the dinuclear cyanido-bridged complexes was found to depend on the molar ratio of $[MN^*_3]$ and KCN and the mode of crystallization. Cooling a 1:3:1 mixture of $[MN^*_3]$, KCN, and 18-crown-6 in toluene led to bright yellow crystals of $[K(18\text{-crown-}6)][CeN^*_3(CN)]\cdot$toluene (**1′a**·toluene) and dark blue crystals of the uranium counterpart **1′b**·toluene, while blue-black crystals of $[K(18\text{-crown-}6)][(UN^*_3)_2(\mu\text{-CN})]$ (**2′b**) were grown by slow diffusion of pentane into a 1:5:1 mixture of $[UN^*_3]$, KCN, and 18-crown-6 in toluene. Not surprisingly, addition of 0.5 mol equiv of NEt_4CN to $[MN^*_3]$ in THF or toluene gave either a pale yellow powder of $[NEt_4][(CeN^*_3)_2(\mu\text{-CN})]$ (**2a**) or a dark blue powder of the uranium analogue **2b**, in 40% and 86% yield, respectively, after usual work-up. Complexes **2a** and **2b** were alternatively isolated in 55% and 79% yield from the comproportionation reactions of $[MN^*_3]$ and $[NEt_4][MN^*_3(CN)]$ (M = Ce, U) in toluene.

Views of the structures of the discrete anion $[(CeN^*_3)_2(\mu\text{-CN})]^-$ of **2′a** and the 1D coordination polymer $[K(18\text{-crown-}6)][(UN^*_3)_2(\mu\text{-CN})]$ (**2′b**) are shown in Figures 1 and 2,

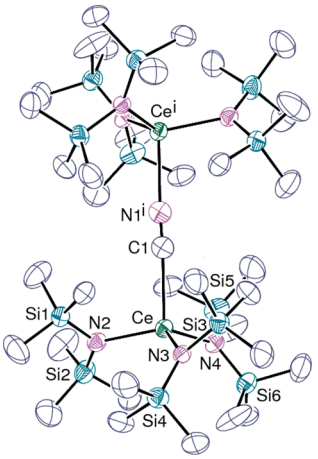

Figure 1. View of the anion $[(CeN^*_3)_2(\mu\text{-CN})]^-$ in **2′a**. Hydrogen atoms are omitted. Displacement ellipsoids are drawn at the 50% probability level. Symmetry code: i = 2 − *x*, *y*, $^1/_2$ − *z*. The cyanide ion is disordered over the two possible positions.

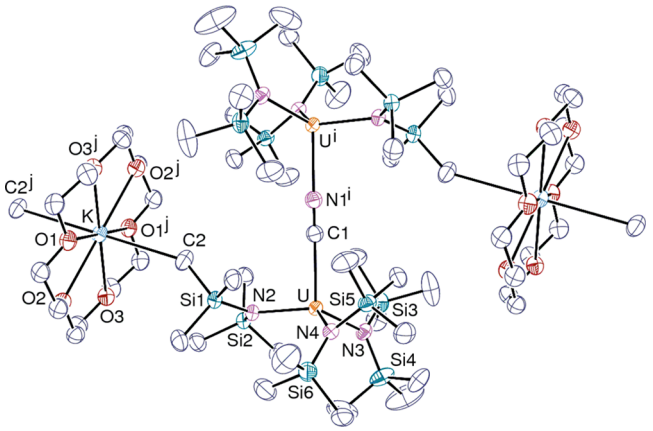

Figure 2. View of the 1D coordination polymer $[K(18\text{-crown-}6)][(UN^*_3)_2(\mu\text{-CN})]$ (**2′b**). Hydrogen atoms are omitted. Displacement ellipsoids are drawn at the 50% probability level. Symmetry codes: i = 1 − *x*, 1 − *y*, 1 − *z*; j = −*x*, −*y*, 1 − *z*. The cyanide ion is disordered over the two possible positions.

respectively, while selected bond distances and angles are listed in Table 1. In these two compounds, the cyanide ion is necessarily disordered, the two atoms being related to one another by a 2-fold rotation axis (**2′a**) or an inversion center (**2′b**). In each $(MN^*_3)_2(\mu\text{-CN})$ fragment, the metal ion is in a distorted tetrahedral environment with the C or N atom of the CN ligand lying on the pseudo- (noncrystallographic) 3-fold

dx.doi.org/10.1021/ic500939t | Inorg. Chem. 2014, 53, 6995−7013

Table 1. Selected Bond Lengths (Å) and Angles (deg) in the Cyanido-Bridged Complexes [K(18-crown-6)(THF)$_2$][(CeN*$_3$)$_2$(μ-CN)] (2′a) and [K(18-crown-6)][(UN*$_3$)$_2$(μ-CN)] (2′b)

	2′a (M = Ce)	2′b (M = U)
M−C(1)/N(1)	2.653(3)	2.583(2)
M−N(2)	2.354(2)	2.3772(17)
M−N(3)	2.371(2)	2.369(2)
M−N(4)	2.378(2)	2.3548(18)
C(1)−N(1)	1.159(6)	1.177(4)
K−C(2)		3.310(3)
C(1)/N(1)−M−N(2)	100.72(10)	95.63(6)
C(1)/N(1)−M−N(3)	107.81(9)	115.63(7)
C(1)/N(1)−M−N(4)	104.77(9)	102.71(6)

rotation axis. The Ce and U atoms are displaced from the N2−N3−N4 face by 0.588(2) and 0.5861(10) Å, respectively. The anionic dinuclear moieties of **2′b** are bridged by the cationic fragment K(18-crown-6) through K···CH$_3$ interactions [K−H2*A* = 2.88 Å and K−H2*B* = 2.79 Å, K···C2 3.310(3) Å], leading to zigzag chains running along the [110] axis. While the ionic radius of uranium(III) is larger than that of cerium(III) by 0.015 Å,[29] the Ce−N(N*) and U−N(N*) bond lengths are equal with an average value of 2.367(10) Å and the U−C/N(CN) distance of 2.583(2) Å is 0.07 Å shorter than the Ce−C/N(CN) distance. Such shortening of U−X bonds (X = C, N, S) with respect to a purely ionic model, which was measured in various pairs of analogous uranium(III) and lanthanide(III) complexes,[30] has been attributed to the more covalent character of the uranium−ligand bond. These M−C/N(CN) distances can be compared with those measured in the trivalent complexes [N^{n}Bu$_4$][M(Cp*)$_2$(CN)$_3$],[13] [2.666(6) Å for M = Ce and 2.641(3) Å for M = U] and [U(Cp*)$_2$(μ-CN)-(^{t}BuNC)]$_3$ [2.61(3) Å],[12] and the cyanide-bridged uranium(IV) compounds [U(Cp*)$_2$(DMF)$_3$(μ-NC)$_2$(AgI)$_2$]$_\infty$ [2.529(2) Å],[8] and [{U(Cp*)$_2$Cl$_2$(μ-CN)}$_2$Mg(THF)$_4$] [2.591(11) Å].[8] The M−N(N*) distances are unexceptional.[31]

The dinuclear fragment of **2b** is retained in solution as shown by the ^{1}H NMR spectrum in THF-d_8 which exhibits at 20 °C two signals of equal intensities at δ_H −9.54 and −10.07, attributed to the SiMe$_3$ groups of the distinct UN*$_3$ moieties which are linked either to the C or N atom of the CN bridge. Broadening of these signals occurred upon cooling the solution down to −90 °C, but well-resolved spectra with splitting of these resonances reflecting the distinct environment of the *endo* and *exo* SiMe$_3$ groups of each MN*$_3$ fragment were not observed. However, the four expected signals are visible on the ^{13}C NMR spectrum of **2b** in THF-d_8 at 20 °C, at δ_C −101.8, −102.5, −104.7, and −105.6. The single signal corresponding to the SiMe$_3$ groups of the cerium counterpart **2a**, visible at δ_H −2.60 on the ^{1}H NMR spectrum at 20 °C, was separated into two peaks of equal intensities at δ_H −3.27 and −3.38 at −20 °C; here again, broadening of these peaks was observed at lower temperatures, but the slow-limit spectrum was not attained.

Solutions of equimolar mixtures of (a) [NEt$_4$][(CeN*$_3$)$_2$(μ-CN)] (**2a**) and the uranium counterpart **2b**, (b) [NEt$_4$]-[CeN*$_3$(CN)] (**1a^{Et}**) and [UN*$_3$], (c) **1b^{Et}** and [CeN*$_3$], or (d) [UN*$_3$], [CeN*$_3$], and NEt$_4$CN in THF exhibited the same ^{1}H NMR spectrum showing four signals located between those of **2a** and **2b**, which were attributed to the mixed cerium(III)/uranium(III) cyanide bridged complexes [NEt$_4$]-[(CeN*$_3$)(μ-CN)(UN*$_3$)] and [NEt$_4$][(CeN*$_3$)(μ-NC)-(UN*$_3$)] (eq 1).

$$\underset{\mathbf{1a^{Et}}}{[NEt_4][(CeN^*_3)_2(\mu\text{-}CN)]} + \underset{\mathbf{1b^{Et}}}{[NEt_4][(UN^*_3)_2(\mu\text{-}CN)]} \rightleftarrows 2[NEt_4][(CeN^*_3)(\mu\text{-}CN/NC)(UN^*_3)] \quad (1)$$

These signals were divided into two pairs of equal intensity corresponding to the CeN*$_3$ and UN*$_3$ fragments. The two signals in each pair, in the 1:4 intensity ratio, would correspond to the SiMe$_3$ groups of the MN*$_3$ fragments linked either to the C or N atom of the CN bridge, as observed for **2a** and **2b**. In view of the better affinity of uranium(III) than cerium(III) for the cyanide coordination mode (vide infra), it is likely that the N*$_3$Ce−NC−UN*$_3$ linkage is preferred over N*$_3$Ce−CN−UN*$_3$. Integration of the spectra indicated that **2a**, **2b**, and the heterodinuclear complexes were in the 1:1:2 molar ratio, in line with a statistical distribution of the MN*$_3$ fragments. Spin saturation transfer experiments[32] as well as addition of **2a** or **2b** to the above mixtures showed that the three dinuclear complexes were in slow equilibrium.

The toluene solvates of the mono(cyanide) complexes **1′a** and **1′b** are isomorphous; a view of the cerium compound is shown in Figure 3, and selected bond distances and angles are

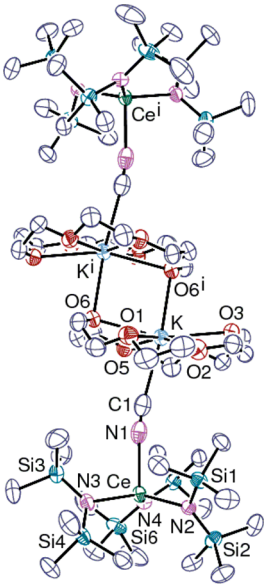

Figure 3. View of the tetranuclear assembly in [K(18-crown-6)][CeN*$_3$(CN)] (**1′a**). Solvent molecules and hydrogen atoms are omitted. Displacement ellipsoids are drawn at the 50% probability level. Symmetry code: i = 1 − *x*, 1 − *y*, 2 − *z*.

listed in Table 2. The structure consists of a centrosymmetric tetranuclear assembly in which the potassium center of each monomeric unit [MN*$_3$(μ-CN)K(18-crown-6)] is coordinated to the O6 atom of the adjacent 18-crown-6 ligand. Such face to face stacking of 18-crown-6 rings is not uncommon,[33] and the average K—O6 distance of 2.83(2) Å in **1′a** and **1′b** can be compared with that of 3.0(1) Å in [K(18-crown-6)OSiPh$_3$]$_2$.[33a] The Ce and U atoms are closer to the N2—N3—N4 face than in **2′a** and **2′b**, with distances of 0.3944(11) and 0.3702(12) Å, respectively. The good quality of the structure of **1′a** permits us to determine the isocyanide bonding mode of the CN ligand as being the more probable one (see Experimental Section), as observed in cyanido−metalate complexes where the lanthanide

dx.doi.org/10.1021/ic500939t | *Inorg. Chem.* 2014, 53, 6995−7013

Table 2. Selected Bond Lengths (Å) and Angles (deg) in the Mono(cyanide) Complexes [K(18-crown-6)][MN*$_3$(CN)]·toluene (M = Ce, 1′a·toluene; M = U, 1′b·toluene)[a]

	1′a·toluene (M = Ce)	1′b·toluene (M = U)
M–N(1)	2.503(3)	2.501(3)
M–N(2)	2.3787(17)	2.366(2)
M–N(3)	2.3767(18)	2.363(2)
M–N(4)	2.3762(17)	2.372(2)
C(1)–N(1)	1.1075(18)	1.159(4)
K–C(1)	2.861(3)	2.835(3)
K–O(6)	2.8555(17)	2.8536(18)
K–O(6^i)	2.8153(17)	2.822(2)
N(1)–M–N(2)	101.29(7)	100.09(8)
N(1)–M–N(3)	95.81(7)	96.33(8)
N(1)–M–N(4)	101.65(7)	100.64(8)
M–N(1)–C(1)	171.3(2)	175.0(2)
K–C(1)–N(1)	172.4(2)	169.6(2)

[a]Symmetry code: i = 1 − x, 1 − y, 2 − z.

ion is the harder site of the Ln—N≡C—M linkage.[15] The Ce—N1 distance of 2.503(3) Å and Ce—N1—C1 angle of 171.3(2)° can be compared with those of 2.579(2) Å and 163.0(2)° in [Ce(dmf)$_4$(H$_2$O)$_3$(μ-NC)Co(CN)$_5$]·H$_2$O,[34] where the Ce atom is 8-coordinate and more sterically crowded. The K—C1 distance of 2.861(3) Å is slightly larger than that of 2.75 Å in [K(18-crown-6)][Me$_3$SnCl(μ-NC)].[35]

From the above results and as previously observed,[8,21,22] the use of countercations such as K$^+$ or Mg^{2+} should be avoided for the formation of anionic species with terminal cyanide ligands. In order to eventually characterize the anionic mono(cyanide) complex [MN*$_3$(CN)]$^-$ with a terminal CN ligand, attempts were made to crystallize the NMe$_4^+$ salt. Solutions of equimolar mixtures of [MN*$_3$] (M = Ce, U) and NMe$_4$CN in toluene/pentane or diethyl ether/pentane deposited colorless crystals of [NMe$_4$][CeN*$_3$(CN)] (**1a^{Me}**) and dark blue crystals of [NMe$_4$][UN*$_3$(CN)] (**1b^{Me}**). Crystals of **1a^{Me}** and **1b^{Me}** are isomorphous; a view of one of the two independent and quite identical anions [UN*$_3$(CN)]$^-$ of **1b^{Me}** is shown in Figure 4, and selected bond distances and angles are listed in Table 3. Although the C and N atoms of the cyanide ions were located so as to give the most satisfying set of refined displacement parameters [Ce(1)–N(1)–C(1) and Ce(2)–C(20)–N(5), U(1)–C(1)–N(1) and U(2)–C(20)–N(5)], their location

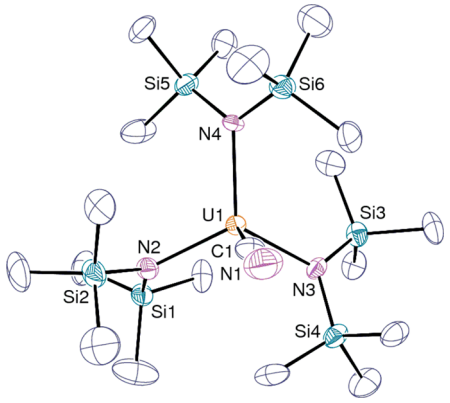

Figure 4. View of one of the two independent anions [UN*$_3$(CN)]$^-$ in **1b^{Me}**. Hydrogen atoms are omitted. Displacement ellipsoids are drawn at the 30% probability level.

remains quite ambiguous due to the moderate crystal quality, and cannot be discussed with confidence. The geometrical parameters of the isolated anions are quite similar to those found in the binuclear cyanido bridged compounds **1′a**·toluene and **1′b**·toluene, and **2′a** and **2′b**. The most notable difference is the distance of the metal center from the mean plane defined by the three nitrogen atoms of the N* ligands (ca. 0.47 Å) which is intermediate between those measured in **1′a/b** and **2′a/b**.

The infrared spectra of **1a** and **1b** show strong absorption bands assigned to the ν(CN) stretching frequencies at 2063 and 2057 cm^{-1}, respectively, while the IR vibrational frequency of the cyanide ion in NEt$_4$CN is 2050 cm^{-1}. These values can be compared with those of [N^{n}Bu$_4$]$_2$[M(Cp*)$_2$(CN)$_3$] (2086 and 2065 cm^{-1} for M = Ce, 2091 and 2060 cm^{-1} for M = U),[13] and those of the mononuclear uranium(IV) compounds [NEt$_4$][U(Cp*)$_2$(CN)$_3$] (2053 and 2188 cm^{-1}),[19] [NR$_4$]$_3$[U(Cp*)$_2$(CN)$_5$] (2091 cm^{-1}),[19] and [U(C$_5$^{t}Bu$_3$H$_2$)$_2$(CN)(OSiMe$_3$)] (2040 cm^{-1}),[17] and they suggest the absence of π back-bonding from the M^{3+} ion to the cyanide ligand.[36a] Compounds **2a** and **2b** display a strong absorption band in the ν(CN) frequency range at 2108 and 2096 cm^{-1}. As expected for bridging CN groups,[36] these values are larger than those corresponding to terminal cyanide ligands in **1a** and **1b**, and they are close to those in [U(Cp)$_2$(CN)] (2112 cm^{-1}),[1] [U(Cp)$_3$(CN)] (2110 or 2116 cm^{-1}),[3,6] [U(C$_5$H$_4$SiMe$_3$)$_3$(CN)] (2088 and 2078 cm^{-1}),[7,8] [U(C$_5$H$_4$^{t}Bu)$_3$(CN)] (2115 and 2108 cm^{-1}),[7,8] and [Ln(Cp)$_2$(CN)] (2187 and 2116 cm^{-1} for Ln = Nd; 2198 and 2136 cm^{-1} for Ln = Yb),[3] which likely possess a polymeric structure with CN bridges.

Bis- and Tris(cyanide) Complexes [M′]$_2$[MN*$_3$(CN)$_2$] and [M′]$_2$[MN*$_2$(CN)$_3$]. The mono(cyanide) complexes **1a** and **1b** were found to be inert in the presence of an excess of NEt$_4$CN in THF at 20 °C. Changing NEt$_4$CN for the more soluble N^{n}Bu$_4$CN led to the ready formation of the bis(cyanide) compounds [N^{n}Bu$_4$]$_2$[MN*$_3$(CN)$_2$] (M = Ce, **3a**; M = U, **3b**). Complexes **3a** and **3b** were isolated, respectively, as an off-white and a bright blue powder in 41% and 55% yield from the reactions of [MN*$_3$] with 2 mol equiv of the ammonium salt. The potassium salts of the anionic bis(cyanide) complexes [K(18-crown-6)]$_2$[MN*$_3$(CN)$_2$] (M = Ce, **3′a**; M = U, **3′b**) were prepared in 34% and 33% yield by reaction of [MN*$_3$] with 2 or 3 mol equiv of KCN in the presence of 2 mol equiv of 18-crown-6 in THF.

The ^{1}H NMR spectra revealed that the bis(cyanide) complexes **3** were in equilibrium with the mono(cyanide)s **1**. For example, the spectrum of a solution of [K(18-crown-6)]$_2$[UN*$_3$(CN)$_2$] (**3′b**) in THF-d_8 exhibits at 20 °C a broad signal at δ_H −5.63 which is split at 10 °C into two peaks at δ_H −3.75 and −5.90 corresponding to the SiMe$_3$ resonances of **3′b** and **1′b**, respectively. The formation constant of **3′b** ($K_{3'b}$) from **1′b** at 10 °C is equal to 5(1) × 10^{-3}; the linear dependence of Ln$K_{3'b}$ versus 1/T allowed the determination of the thermodynamic parameters $-\Delta H_{3'b}$ = 104(2) kJ mol^{-1} and $-\Delta S_{3'b}$ = 330(5) J mol^{-1} K^{-1}. The analysis of the equilibrium in the cerium counterparts **3′a** and **1′a** was prevented by the overlap of the SiMe$_3$ signals.

Crystals of **3a** suitable for X-ray diffraction were obtained by crystallization from a mixture of tetrahydrofuran and diethyl ether. Crystals of **3′a** and **3′b** were grown upon slow diffusion of pentane into a 1:5:2 mixture of [MN*$_3$], KCN, and 18-crown-6 in THF or toluene, and crystallization from benzene afforded crystals of the solvates **3′a**·2benzene and **3′b**·

dx.doi.org/10.1021/ic500939t | Inorg. Chem. 2014, 53, 6995−7013

Table 3. Selected Bond Lengths (Å) and Angles (deg) in the Mono(cyanide) Complexes $[NMe_4][MN^*_3(CN)]$ (M = Ce, $\mathbf{1a^{Me}}$; and U, $\mathbf{1b^{Me}}$)

$\mathbf{1a^{Me}}$		$\mathbf{1b^{Me}}$			$\mathbf{1a^{Me}}$	$\mathbf{1b^{Me}}$
Ce(1)−N(1)	2.516(11)	U(1)−C(1)	2.455(15)	M(2)−C(20)	2.547(10)	2.604(14)
Ce(1)−N(2)	2.367(7)	U(1)−N(2)	2.354(10)	M(2)−N(6)	2.371(7)	2.343(9)
Ce(1)−N(3)	2.369(5)	U(1)−N(3)	2.344(7)	M(2)−N(7)	2.367(5)	2.348(7)
Ce(1)−N(4)	2.366(7)	U(1)−N(4)	2.343(8)	M(2)−N(8)	2.385(6)	2.357(9)
N(1)−C(1)	1.151(15)	N(1)−C(1)	1.17(2)	N(5)−C(20)	1.140(14)	1.161(18)
N(1)−Ce(1)−N(2)	104.3(3)	C(1)−U(1)−N(2)	102.8(4)	C(20)−M(2)−N(6)	102.9(3)	104.6(4)
N(1)−Ce(1)−N(3)	99.3(2)	C(1)−U(1)−N(3)	100.2(4)	C(20)−M(2)−N(7)	104.8(2)	102.9(3)
N(1)−Ce(1)−N(4)	100.3(3)	C(1)−U(1)−N(4)	100.4(4)	C(20)−M(2)−N(8)	97.7(3)	98.0(4)

2benzene. Views of the discrete dianion $[CeN^*_3(NC)_2]^{2-}$ of **3a**, the 1D chain of **3′a**, and the trinuclear complex **3′a**·2benzene are presented in Figures 5−7, respectively, and

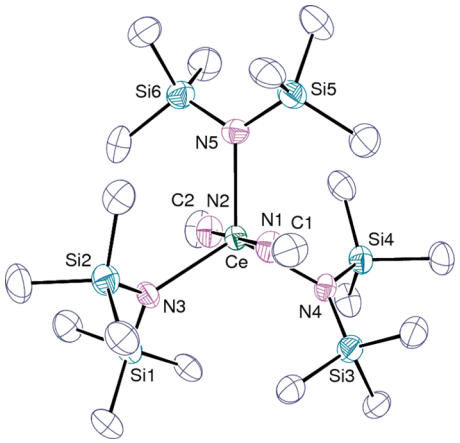

Figure 5. View of the dianion $[CeN^*_3(NC)_2]^{2-}$ in **3a**. Hydrogen atoms are omitted. Displacement ellipsoids are drawn at the 30% probability level.

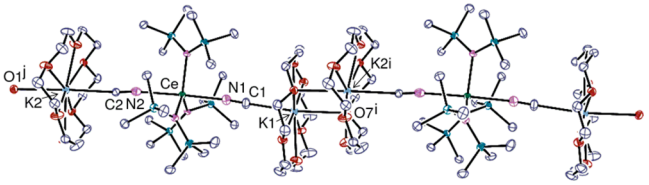

Figure 6. View of the 1D polymer $[K(18\text{-crown-}6)]_2[CeN^*_3(NC)_2]$ (**3′a**). Hydrogen atoms are omitted. Displacement ellipsoids are drawn at the 30% probability level. Symmetry codes: i = $x-1, y, z-1$; j = $x+1, y, z+1$.

selected bond distances and angles are listed in Table 4. The $CeN^*_3(NC)_2$ fragment is present in the three structures, with the cerium atom in a quite perfect trigonal bipyramidal environment defined by the nitrogen atoms of the N* ligands and the N atoms of the NC ligands which are in the apical positions. The isocyanide bonding mode is quite unambiguously determined in **3a** and **3′a**·2benzene, as well as for one ligand in **3′a** (the second one being compatible with both possibilities). The Ce−N(NC) distances vary from 2.569(6) to 2.673(3) Å, with a mean value of 2.60(4) Å whereas the Ce−N(N*) bond lengths are in the range 2.393(5)−2.423(5) Å and average 2.41(1) Å. The Ce−N(NC) and Ce−N(N*) bonds are longer than in the mono(cyanide) **1′a**, by ∼0.1 and ∼0.03 Å respectively; these differences reflect the increase of charge and coordination number from **1′a** to **3′a**, but the larger

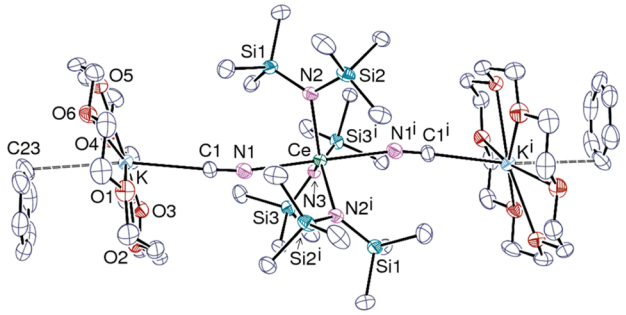

Figure 7. View of $[K(18\text{-crown-}6)]_2[CeN^*_3(NC)_2]$·2benzene (**3′a**·2benzene). Hydrogen atoms are omitted. Displacement ellipsoids are drawn at the 30% probability level. Symmetry code: i = $1-x, y, {}^3/_2-z$.

lengthening of the Ce−N(NC) bond could suggest that the NC ligand is less strongly bound in **3′a** than in **1′a**. In complexes **3′a** and **3′a**·2benzene, the NC ligand is in bridging position between the Ce and K atoms, and the average K−C distance of 2.86(3) Å is identical to that found in **1′a**. The polymeric structure of **3′a** which is isomorphous with that of the carbonyl compound $[K(18\text{-crown-}6)]_2[YN^*_3(CO)_2]$,[37] arises from the presence of interactions between adjacent K(18-crown-6) fragments (K1−O7^i and K2−O1^j), while polymer formation is disrupted by interactions with the benzene solvent molecules in **3′a**·2benzene, in which the shortest distance of 3.441(2) Å between K and the carbon atom C23 of C_6H_6 is similar to that of 3.423(4) Å for the η^1-coordinated toluene in $[Er(\eta^2\text{-}^t\mathrm{Bu}_2\mathrm{pz})_4][K(18\text{-crown-}6)(DME)(toluene)]$.[38] Crystals of **3′b** and **3′b**·2benzene are isomorphous with those of the cerium counterparts but not isostructural since the cyanide bonding mode of the CN ligand could be unambiguously determined. Views of **3′b** and of **3′b**·2benzene are shown in Figures 8 and 9, respectively, and selected bond distances and angles are listed in Table 4. The average U−C distance of 2.62(3) Å is identical to that of 2.639(4) in $[N^n\mathrm{Bu}_4]_2[U(Cp^*)_2(CN)_3]$.[13] The striking difference between the isocyanide and cyanide ligation modes of the CN ligand in the cerium and uranium complexes **3′a** and **3′b** can be explained by the U^{III} ion being softer than the Ce^{III} ion in the HSAB classification and having a greater affinity for the softer carbon end of the CN ligand. The distinct nature of the Ce−N and U−C bonding in **3′a** and **3′b** has been analyzed by DFT calculations (vide infra).

In addition to their equilibrium with the mono(cyanide)s **1**, new facts on the behavior of the bis(cyanide) complexes **3** in solution emerged from the ^{1}H NMR spectra after several hours. Complex **3a** was completely transformed, after 15 h at 20 °C in THF, into the equimolar mixture of $[N^n\mathrm{Bu}_4]N^*$, which likely

dx.doi.org/10.1021/ic500939t | Inorg. Chem. 2014, 53, 6995−7013

Table 4. Selected Bond Lengths (Å) and Angles (deg) in the Bis(cyanide) Complexes $[N^nBu_4]_2[CeN^*_3(CN)_2]$ (3a), $[K(18\text{-crown-6})]_2[MN^*_3(CN)_2]$ (M = Ce, 3′a; M = U, 3′b), and $[K(18\text{-crown-6})]_2[MN^*_3(CN)_2]\cdot 2$benzene (M = Ce, 3′a·2benzene; M = U, 3′b·2benzene)[a]

	3a	3′a	3′b		3′a·2benzene	3′b·2benzene
Ce−N(1)	2.569(6)	2.579(3)		Ce−N(1)	2.596(2)	
U−C(1)			2.578(7)	U−C(1)		2.617(3)
Ce−N(2)	2.574(6)	2.673(3)		M−N(2)	2.4127(16)	2.3967(19)
U−C(2)			2.662(7)	M−N(3)	2.410(2)	2.390(3)
M−N(3)	2.412(5)	2.3984(18)	2.377(4)	C(1)−N(1)	1.161(3)	1.164(3)
M−N(4)	2.423(5)	2.408(2)	2.384(4)	K−C(1)	2.863(2)	
M−N(5)	2.393(5)	2.420(2)	2.397(4)	K−N(1)		2.805(3)
C(1)−N(1)	1.169(8)	1.156(3)	1.171(7)	K−C(23)	3.441(2)	3.459(2)
C(2)−N(2)	1.137(9)	1.163(3)	1.165(7)	N(1)−Ce−N(1^i)	175.38(9)	
K(1)−C(1)		2.819(3)		C(1)−U−C(1^i)		174.90(10)
K(1)−N(1)			2.778(7)	N(2)−M−N(2^i)	119.73(8)	120.03(9)
K(2)−C(2)		2.887(3)		N(2)−M−N(3)	120.13(4)	119.98(4)
K(2)−N(2)			2.858(6)			
K(1)−O(7^i)		3.0151(18)	3.032(4)			
K(2)−O(1^j)		2.9923(18)	3.005(4)			
N(1)−Ce−N(2)	177.33(19)	176.93(7)				
C(1)−U−C(2)			176.34(19)			
N(3)−M−N(4)	120.20(18)	116.71(7)	116.96(15)			
N(3)−M−N(5)	119.30(18)	124.04(7)	123.33(15)			
N(4)−M−N(5)	119.87(18)	119.11(7)	119.54(15)			

[a]Symmetry codes. 3′a and 3′b: i = $x-1$, y, $z-1$; j = $x+1$, y, $z+1$. 3′a·2benzene and 3′b·2benzene: i = $1-x$, y, $1.5-z$.

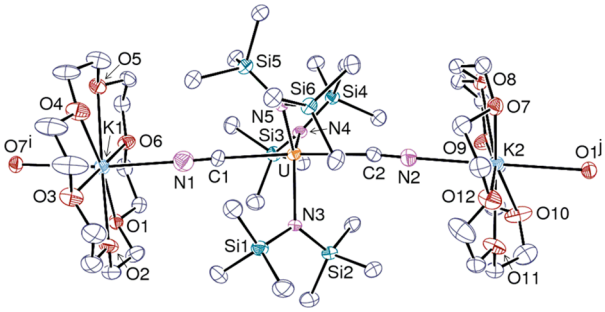

Figure 8. View of $[K(18\text{-crown-6})]_2[UN^*_3(CN)_2]$ (3′b). Hydrogen atoms are omitted. Displacement ellipsoids are drawn at the 30% probability level. Symmetry codes: i = $x-1$, y, $z-1$; j = $x+1$, y, $z+1$.

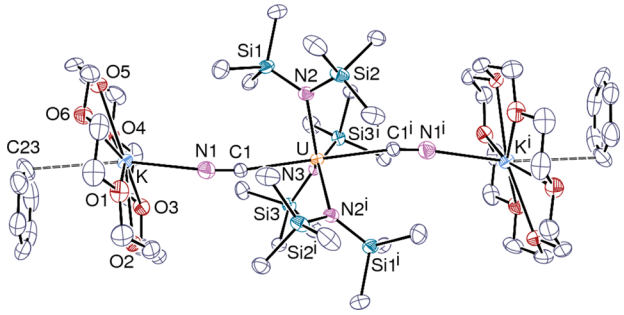

Figure 9. View of $[K(18\text{-crown-6})]_2[UN^*_3(CN)_2]\cdot 2$benzene (3′b·2benzene). Hydrogen atoms are omitted. Displacement ellipsoids are drawn at the 30% probability level. Symmetry code: i = $1-x$, y, $^3/_2-z$.

underwent a Hoffman elimination in the reaction mixture, the mono(cyanide) **1a** and the tris(cyanide) $[N^nBu_4]_2[CeN^*_2(CN)_3]$ (**4a**), characterized by its $SiMe_3$ signal at δ_H −4.10. The uranium counterpart $[N^nBu_4]_2[UN^*_2(CN)_3]$ (**4b**) was similarly obtained together with **1b** from **3b** after 3 days at 20 °C; its $SiMe_3$ signal is visible at δ_H −6.81. Complexes **4a** and **4b** were synthesized on a preparative scale from $[MN^*_3]$ and 2 mol equiv of N^nBu_4CN, and after elimination of **1a** or **1b** by extraction in a mixture of THF and diethyl ether, were isolated as an off-white or black blue powder in 41% and 37% yield, respectively. Complexes **4a** or **4b** clearly derived from **3a** or **3b** by the replacement of a N* ligand with a CN group released in the equilibrium between **3a** or **3b** and **1a** or **1b** (eqs 2 and 3).

$$[M'][MN^*_3(CN)] + M'CN \rightleftarrows [M']_2[MN^*_3(CN)_2] \quad (2)$$
(1) (3)

$$2[M']_2[MN^*_3(CN)_2] \rightarrow [M'][MN^*_3(CN)] + [M']_2[MN^*_2(CN)_3] + M'N^* \quad (3)$$
(3) (1) (4)

Compounds **4a** and **4b** were more readily prepared in the better yields of 63% and 59% yield, respectively, directly from $[MN^*_3]$ (M = Ce, U) by treatment with 3 mol equiv of N^nBu_4CN. Crystallization of **4a** from THF gave colorless crystals with bluish reflection of **4a**·0.5THF while black crystals of **4b**·Et_2O were obtained by crystallization from a mixture of THF and diethyl ether.

A view of the dianion of one of the two independent and quite identical complexes of **4a** and the dianion of **4b** are shown in Figures 10 and 11, respectively, while selected bond distances and angles are presented in Table 5. The crystal structure of **4b** is of better quality than that of **4a**, and it indicates the cyanide coordination mode of the CN ligand. The metal centers are in a distorted trigonal bipyramidal configuration, with the basis defined by the N atoms of the N* ligands and the C or N atom of the central CN group, with the C or N atoms of the lateral CN ligands being in apical

dx.doi.org/10.1021/ic500939t | Inorg. Chem. 2014, 53, 6995−7013

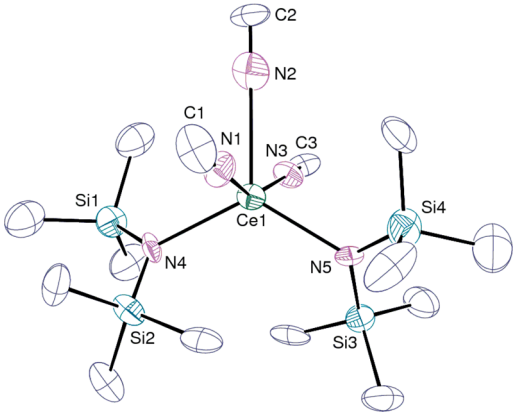

Figure 10. View of one of the two independent dianions $[CeN^*_2(NC)_3]^{2-}$ in **4a**. Hydrogen atoms are omitted. Displacement ellipsoids are drawn at the 30% probability level.

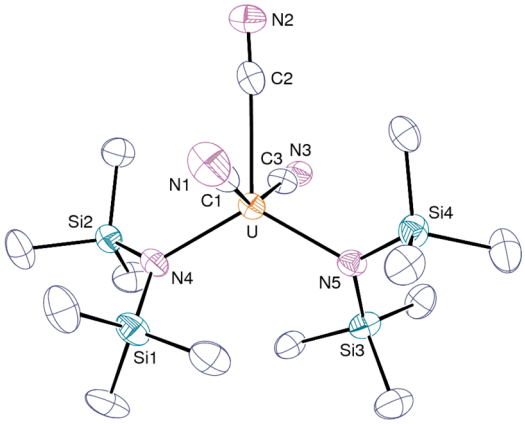

Figure 11. View of the dianion $[UN^*_2(CN)_3]^{2-}$ in **4b**. Hydrogen atoms are omitted. Displacement ellipsoids are drawn at the 30% probability level.

positions. The structure resembles that of **3′a** and **3′b**, with one of the N* ligands being replaced with a CN group. The U−C and M−N bonds are quite identical to those measured in complexes **3′a** and **3′b**.

The infrared spectra of the cerium compounds **3a**, **3′a**, and **4a** show strong absorption bands assigned to the ν_s(CN) and ν_{as}(CN) stretching frequencies at 2074 and 2173, 2078 and 2171, and 2065 and 2175 cm^{-1}, respectively, which are again larger than those of the corresponding uranium complexes **3b**, **3′b**, and **4b**, at 2058 and 2197, 2063 and 2091, and 2059 and 2179 cm^{-1}, respectively. These frequencies do not permit distinguishing the isocyanide and cyanide bonding modes of the CN ligands in **3a** and **3b**, as previously found for the identical values of ν(CN) in the tetravalent thorium and uranium complexes $[Th(C_5{}^tBu_3H_2)_2(NC)(OSiMe_3)]$ (2039 cm^{-1})[18] and $[U(C_5{}^tBu_3H_2)_2(CN)(OSiMe_3)]$ (2040 cm^{-1}).[17]

Molecular Geometry Optimization of the Bis(cyanide) Complexes. In order to discuss the bonding of the cyanide or isocyanide groups to the MN^*_3 metallic moieties, we first consider the two complexes $[MN^*_3(CN)_2]^{2-}$ and $[MN^*_3(NC)_2]^{2-}$ (M = Ce, U). The computed bond lengths M−CN/NC, M−N*, and C−N of the DFT optimized structures (Figure 12) are reported in Table 6 for the $[CeN^*_3(CN)_2]^{2-}$

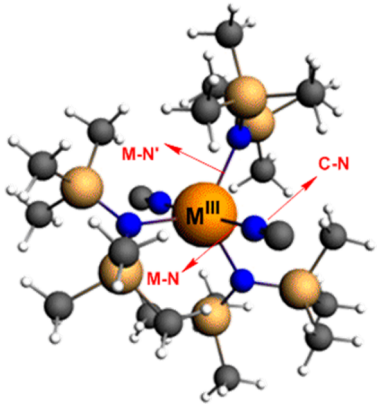

Figure 12. DFT/ZORA $[MN^*_3(NC)_2]^{2-}$ optimized geometry.

and $[UN^*_3(NC)_2]^{2-}$ actual complexes **3′a** and **3′b**, and their hypothetical isomers $[UN^*_3(NC)_2]^{2-}$ and $[CeN^*_3(CN)_2]^{2-}$ using the three GGA functionals, i.e., BP86, PW91, and PBE. These theoretical results can be compared with the crystallographic data of **3′a** and **3′b**. First of all, it can be seen that the different DFT functionals used lead to similar optimized bond distances. However, as previously observed,[39] the ZORA/BP86/TZP computed geometries are in slightly better agreement with the metal−ligand bond lengths determined by X-ray diffraction in the cases of uranium−cyanide U−CN and cerium−isocyanide Ce−NC coordination. It is noteworthy

Table 5. Selected Bond Lengths (Å) and Angles (deg) in the Tris(cyanide) Complexes $[N^nBu_4]_2[CeN^*_2(CN)_3]\cdot 0.5THF$ (4a·0.5THF) and $[N^nBu_4]_2[UN^*_2(CN)_3]\cdot Et_2O$ (4b·Et_2O)

4a·0.5THF[a]				4b·Et_2O	
Ce(1)−N(1)	2.550(13)	Ce(2)−N(6)	2.573(13)	U−C(1)	2.568(11)
Ce(1)−N(2)	2.627(14)	Ce(2)−N(7)	2.641(14)	U−C(2)	2.594(10)
Ce(1)−N(3)	2.564(14)	Ce(2)−N(8)	2.624(16)	U−C(3)	2.639(9)
Ce(1)−N(4)	2.385(10)	Ce(2)−N(9)	2.363(12)	U−N(4)	2.332(7)
Ce(1)−N(5)	2.395(12)	Ce(2)−N(10)	2.310(12)	U−N(5)	2.336(7)
N(1)−C(1)	1.243(18)	N(6)−C(16)	1.120(15)	N(1)−C(1)	1.099(13)
N(2)−C(2)	1.158(15)	N(7)−C(17)	1.152(14)	N(2)−C(2)	1.194(12)
N(3)−C(3)	1.093(17)	N(8)−C(18)	1.124(17)	N(3)−C(3)	1.143(11)
N(1)−Ce(1)−N(3)	156.3(4)	N(6)−Ce(2)−N(8)	157.4(3)	C(1)−U−C(3)	155.2(3)
N(2)−Ce(1)−N(4)	116.4(5)	N(7)−Ce(2)−N(9)	121.0(4)	C(2)−U−N(4)	119.6(3)
N(4)−Ce(1)−N(5)	122.3(3)	N(9)−Ce(2)−N(10)	120.0(4)	C(2)−U−N(5)	119.9(3)
N(2)−Ce(1)−N(5)	121.2(5)	N(7)−Ce(2)−N(10)	119.0(5)	N(4)−U−N(5)	120.4(3)

[a]Values for the two independent dianions.

dx.doi.org/10.1021/ic500939t | Inorg. Chem. 2014, 53, 6995−7013

Table 6. Relevant Optimized Averaged Metal−Ligand Bond Distances (Å) and Available X-ray Data

BP86/PW91/PBE	$U(CN)_2$	$Ce(CN)_2$	Δ (Å)[a]
⟨M−C⟩	2.604/2.598/2.600	2.766/2.771/2.771	0.162
X-ray	2.578(7)−2.662(7) ⟨2.62(6)⟩		
⟨C−N⟩	1.180/1.178/1.180	1.176/1.174/1.176	
X-ray	1.165(7)−1.171(7) ⟨1.168⟩		
⟨M−N*⟩	2.378/2.368/2.370	2.487/2.472/2.475	
X-ray	2.377(4)−2.397(4) ⟨2.39(1)⟩		
	$U(NC)_2$	$Ce(NC)_2$	Δ (Å)[a]
⟨M−N⟩	2.483/2.481/2.487	2.606/2.612/2.619	0.123
X-ray		2.579(3)−2.673(3) ⟨2.62(6)⟩	
⟨N−C⟩	1.185/1.183/1.185	1.181/1.179/1.181	
X-ray		1.156(3)−1.163(3) ⟨1.159⟩	
⟨M−N*⟩	2.389/2.375/2.375	2.491/2.479/2.479	
X-ray		2.398(2)−2.420(2) ⟨2.41(1)⟩	

[a]BP86 metric difference between Ce−C/N and U−C/N bond distances.

that the comparison between the two Ce^{III} and U^{III} analogous complexes in Table 6 reveals a significant shortening of the computed metal−ligand bond distances when passing from the cerium to the uranium species, i.e., M−CN in the $M(CN)_2$ species (2.766 for Ce vs 2.604 Å for U, BP86 results) and M−NC in $M(NC)_2$ complexes (2.606 vs 2.483 Å). This bond length shortening is also observed for the metal-amide M−N* coordination and could account for Ln^{III}/An^{III} differentiation. The metric difference Δ (Å) between the Ce−C/N and U−C/N bond distances obtained with ZORA/BP86/TZP is predicted to be larger for the cyanide CN than for the isocyanide NC ligand (0.162 vs 0.123), suggesting that the former leads to a more covalent bonding than the latter, thus explaining in part the distinct coordination of these two ligands toward the Ce^{III} and U^{III} ions, as experimentally observed. The electronic structure study will shed light on these points.

Electronic Structures of the Bis(cyanide) Complexes. As shown in Figure 13, the cyanide and isocyanide ligands are expected to be strong σ-donors, via donation from either the C-localized upper 2σ orbital of CN^- or the lower N-localized 1σ orbital of NC^- with nitrogen major character. In fact, it was reported in previous work on cyanide and isocyanide donation abilities to uranyl UO_2^{2+} dicationic systems that the better energetic matching of the C-localized σ orbital on the cyanide ligand to the $U^{VI}(5f^0)$ metal-based orbitals makes it a much more effective donor than the N-localized σ orbital.[25,40] To further investigate the metal−ligand bonding, NPA and QTAIM electronic structure calculations have been performed considering the optimized geometries of the cyanide and isocyanide systems at the ZORA/BP86/TZP level (see Computational Details).

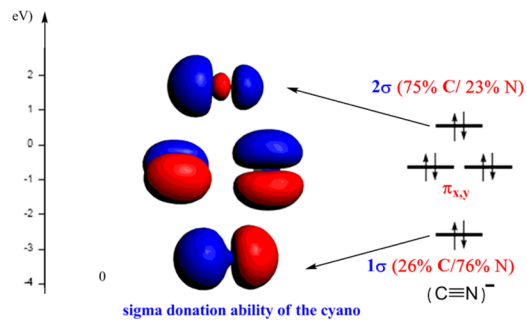

Figure 13. MO diagram of the anionic cyano ligand.

The NPA[41a] and QTAIM[41b] approaches have proved to be more reliable than the Mulliken Population Analysis (MPA),[41c] especially for f-element complexes. Furthermore, as mentioned in the Computational Details, the topological QTAIM method developed by Bader[41b] allows us to probe the covalency in f-element−ligand bonds with results in good agreement with experimental trends,[41d−f] especially considering lanthanide-(III)/actinide(III) differentiation.[41f−h] Both the NPA and QTAIM results for the $[MN^*_3X_2]^{2-}$ complexes (M = Ce, U; X = CN/NC) are given in Table 7. Natural metal, carbon, and nitrogen atomic net charges as well as the metallic spin populations ρ_M are presented; ρ_M is computed as the difference between the total α and β spins electronic populations of the metal. The QTAIM results, i.e., electron (ρ_c) and energy densities (H_c) data, at the metal−ligand bond critical points for M−CN/NC bonds are also listed. Examination of the NPA results indicates small but significantly different metal natural charges for cyanide M−CN and isocyanide M−NC complexes (2.07 vs 2.18 for U) which are consistent with the slightly stronger σ-donation of the cyanide ligand. This difference becomes more pronounced when comparing the two Ce^{III}/U^{III}−CN systems (e.g., 2.39 vs 2.07), which could account for the Ce^{III}/U^{III} differentiation. Comparison of the charge distribution on the CN ligand reveals a much lower C-cyano natural charge in U^{III} than in Ce^{III} species (−0.11 vs −0.54), which sustains its stronger σ-donation for the actinide system. Similarly for the Ce^{III} system, the N-isocyanide donation is stronger than the C-cyanide, the natural charge being significantly lower in the former case (−0.44 for N vs −0.54 for C); this difference contributes to the chosen coordination mode of this species. Interestingly, the total charge of the CN moiety in the case of cyanide coordination, equal to −0.84 and −0.40 for the Ce^{III} and U^{III} complexes, respectively, indicates a more ionic bonding for the former species. Thus, it seems that a covalent factor, presumably slight, likely to originate mainly from the cyano and/or isocyano σ-donation abilities and the better energetic matching between metallic orbitals d/f and ligand orbitals, is partly responsible for the differentiation.

To further assess these factors, BP86/QTAIM data for M−CN/NC metal−ligand bond critical points were computed and showed that the electron densities ρ_c and the energy densities H_c are low, being equal to 0.018 and 0.027 e/Bohr^3 and to

Table 7. ZORA/BP86/TZP NPA and QTAIM Results for the $[MN^*_3X_2]^{2-}$ (M = Ce, U; X = CN/NC) Complexes

	natural spin population		NPA net charges		QTAIM M−C/N	
M−(CN/NC) structure	ρ_M	q_M	C−N	N−C	ρ_c (e/Bohr^3)	H_c
Ce(III) doublet	1.02/1.01	2.39/2.44	−0.54: −0.30	−0.44: −0.01	0.018/0.022	−0.013/−0.016
U(III) quartet	2.88/2.85	2.07/2.18	−0.11: −0.29	−0.40: −0.01	0.027/0.025	−0.026/−0.018

dx.doi.org/10.1021/ic500939t | Inorg. Chem. 2014, 53, 6995−7013

Table 8. ZORA/BP86/TZP Nalewajski–Mrozek (NM) and Mayer Bond Orders Results for the $[MN^*_3X_2]^{2-}$ (M = Ce, U; X = CN/NC) Complexes

		atom–atom bond orders			
		Mayer		NM	
structure M–(CN/NC)	d (Å)	⟨M–C/N⟩	⟨C–N/N–C⟩	⟨M–C/N⟩	⟨C–N/N–C⟩
Ce(III) doublet	2.766/2.606	0.449/0.307	2.858/2.676	0.587/0.577	3.209/3.136
U(III) quartet	2.604/2.483	0.614/0.439	2.814/2.602	0.814/0.778	3.095/3.034

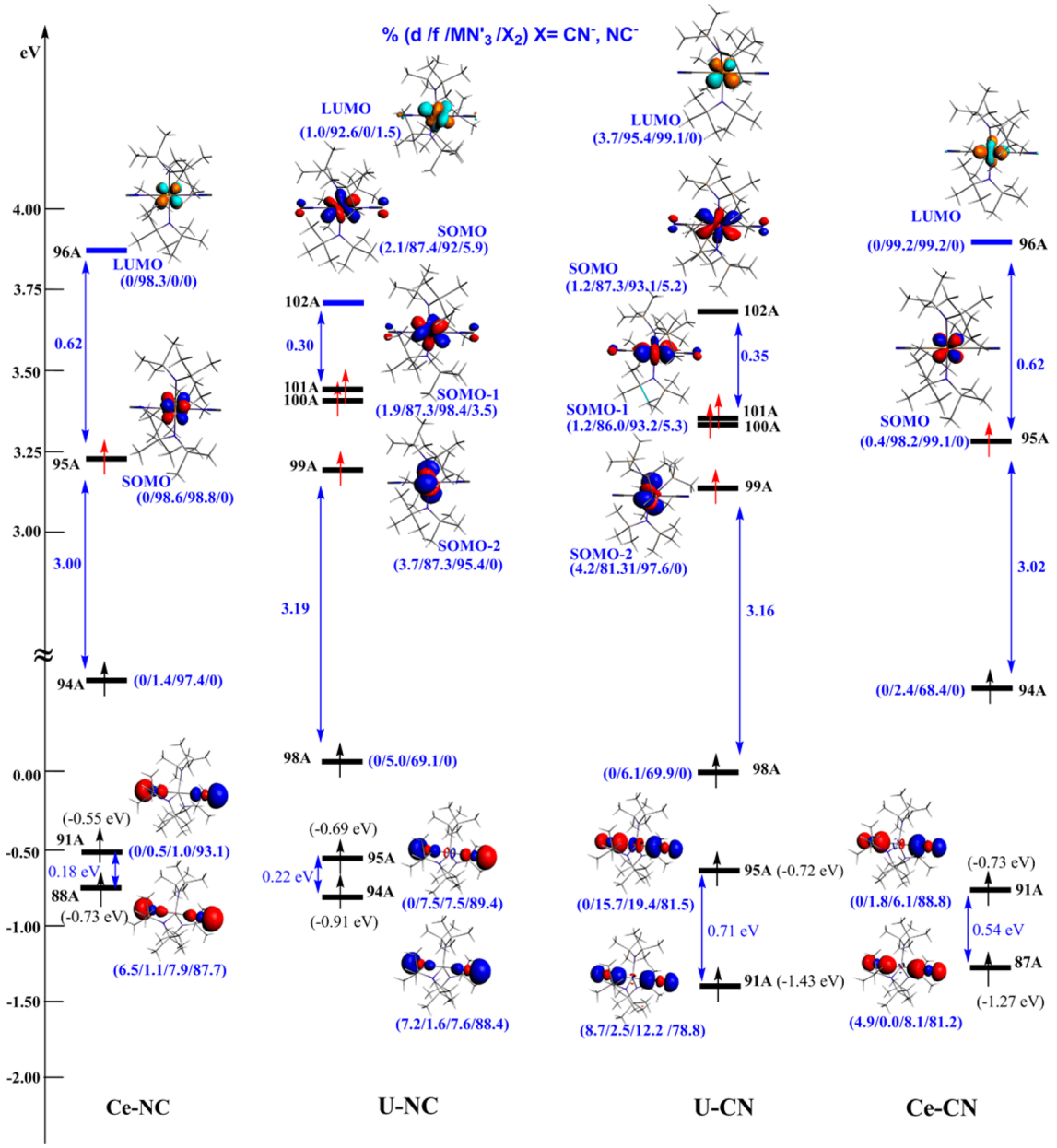

Figure 14. ZORA/BP86/TZP α spin MO diagram for M–CN/NC $[MN^*_3X_2]^{2-}$ complexes. Used cutoff, 0.03 e/Bohr^3.

−0.013 and −0.026 au, for cerium and uranium, respectively. As noted in previous works on f-complexes,[41d,h] these low bond AIM critical point data suggest weak covalency and are indicative of dominant ionic metal–ligand bonding. However, in the case of the Ce^{III}/U^{III} pair, the significant slightly larger values obtained for the actinide complex by comparison with its lanthanide counterpart are likely indicative of a non-negligible covalent character for the actinide–ligand bonding. This is in line with the NPA analysis, and this point is supported by bond order calculations.

The computed Mayer[42d] and Nalewajski–Mrozek (NM)[43a,b] bond indices for the M–N and N–C bonds are reported in Table 8. As expected, NM and Mayer analyses give larger metal–CN/NC bond orders for uranium complexes than for their cerium congeners, correlating well with structural features and NPA and QTAIM results. More interestingly, these bond orders indicate a stronger coordination preference of the cyano

dx.doi.org/10.1021/ic500939t | Inorg. Chem. 2014, 53, 6995–7013

Table 9. Energy Decomposition Analysis at the ZORA/BP86/TZP Level for the $[MN^*_3X_2]^{2-}$ (M = Ce, U; X = CN/NC) Complexes

MX_2	E_{st} (eV)	E_{orb} (eV)	TBE_{frag} (eV)	TBE_{frag} (kcal mol^{-1})	relative stability ΔE (kcal mol^{-1})
$Ce(CN)_2$	−2.129	−3.075	−5.205	−120.0	7.0
$Ce(NC)_2$	−1.879	−3.630	−5.509	−127.0	0.0
$U(CN)_2$	+0.349	−5.846	−5.497	−126.8	0.0
$U(NC)_2$	+0.517	−5.630	−5.112	−117.9	8.9

ligand toward uranium than cerium. This is clearly highlighted by NM descriptors, where a small difference appears between the cyanide Ce−CN and isocyanide Ce−NC bond orders (0.587 vs 0.577), while this difference is more pronounced in the uranium case (0.814 vs 0.778).

Furthermore, the computed frequencies of the stretching modes of vibration for the isocyanide Ce−NC (2048, 2051 cm^{-1}) and cyanide U−CN (2021, 2034 cm^{-1}) ligands, which have been calculated at the ZORA/BP86/TZP level, are in good agreement with experimental data. Indeed, the theoretical ν(CN) stretching frequencies of the cerium(III) complex are slightly larger than those of the corresponding uranium counterpart. The frequency values are in good correlation with the electronic analysis provided by NPA, QTAIM, and bond order schemes (C−N bond order higher for the Ce^{III} than the U^{III} complex) and account once again for the Ln^{III}/An^{III} differentiation. The binding of CN^- or NC^- to the Ce^{III} and U^{III} metallic ions has a slight but significant effect on the stretching frequencies of these ligands. Moreover, as noted by previous works on the difference in CN/NC coordination to uranyl moieties,[25,40] a correlation between a decrease in the frequency values (2048 Ce−NC vs 2021 cm^{-1} U−CN) and the increase of the charge transfer (2.44 Ce vs 2.07 U, NPA results, Table 7), when passing from isocyanide Ce−NC bonding to cyanide U−CN, can be observed. Finally, it is interesting to note that the computed stretching frequencies of the metal−ligand bonds, i.e., ν(M−C/N) for the cyanide and isocyanide systems, reveal a decrease in the frequency value when passing from U^{III} to Ce^{III} complexes. Indeed, the computed symmetric and asymmetric vibration frequencies of the two isocyanide Ce−NC bonds range from 148 to 191 cm^{-1} and are lower than those of the cyanide U−CN bonds (182 to 231 cm^{-1}). This result, which correlates well with the computed bond orders for the two complexes (0.814 for U−CN vs. 0.577 for Ce−NC, see Table 8), certainly indicates slightly stronger metal−ligand bonds for the U^{III} complex. In the same way, we found that the symmetric metal−ligand stretching frequency is higher for the cyanide U−C bond than for the U−N bond of the hypothetical isocyanide complex, i.e., 231 vs 212 cm^{-1}.

Molecular Orbital (MO) Analysis of the Bis(cyanide) Complexes. MO frontier diagrams of the trivalent $[MN^*_3X_2]^{2-}$ complexes (M = Ce or U, X = CN or NC) are displayed in Figure 14. For the sake of simplicity, the α spin MOs only are displayed. In this figure, the percentages %(d/f/MN^*_3/X_2) represent, respectively, the contributions of the d, f orbitals, the MN^*_3 fragment, and the cyanide or isocyanide ligands to the frontier MOs. As displayed in this diagram, two different but significant sets of MOs appear. For all cyanide and isocyanide complexes, the diagram shows that the highest occupied α spin orbitals, i.e., SOMO, SOMO − 1, and SOMO − 2, in U^{III} (f^3) complexes and the SOMO in the Ce^{III} (f^1) counterpart are essentially metallic, with a strong f orbital character as indicated by the percentage orbital composition %(d/f/MN^*_3/X_2). In the case of the U^{III} systems, a weak cyanide or isocyanide ligand contribution of ca. 5% is observed in the SOMO and SOMO − 1; however, no presence of metal-to-ligand π^* back-donation is indicated by these frontier MOs. It is also noteworthy that no π interaction occurs between the central metal and the cyanide or isocyanide MO as the weight of C-localized orbital of CN^- or N-localized orbital of NC^- are zero in percentage. As aforementioned, this confirms the fact that these ligands remain mainly σ donors in character.

The most striking results in the MO diagram are the second sets of MOs with σ donation character which are deeper in energy. In fact, the comparison between the cyanide U−CN and Ce−CN electronic structure reveals that the MN^*_3 orbitals weight is slightly larger for uranium(III) complexes than for their cerium(III) analogues, as can be seen in the σ-donating MOs # 91A and 87A (12.2% vs 8.1%, respectively). This difference is smaller when comparing isocyanide U−NC and Ce−NC pair MO # 94A and 88A (7.6 vs 7.9% respectively). Furthermore, the comparison between Ce and U cyanide complexes shows a greater weight of 6d/5f orbitals in the U−CN interaction than of 5d/4f in the Ce−CN interaction (8.7/2.5% vs 4.9/0.0%). More interestingly, the 5f role is more exalted relative to the 4f one in upper donating σ-MO, i.e., # 95A and 91A (15.7% vs 1.8%) when comparing U^{III} and Ce^{III} systems, respectively. This illustrates the better energy matching and overlap between the actinide 6d/5f orbitals and the C-localized σ-donating orbitals. Turning back to isocyanide systems, the d/f contribution seems to be smaller than in the cyanide cases, as σ donating NC orbitals are deeper in energy and do not interact efficiently with the metallic MN^*_3 moieties. This can be illustrated by the energetic splitting of the two σ donating MO levels which is significantly larger when comparing, for example, cyanide and isocyanide U^{III} systems (0.71 vs 0.22 eV) as for Ce^{III} cases (0.54 vs 0.18 eV). This difference is also greater when comparing cyanide Ce/U systems (0.71 vs 0.54 eV).

As indicated by the electronic structure analysis, the variations in structural parameters of the considered complexes could be explained by the σ-donating abilities of the cyanide and isocyanide ligands and the occurrence of a higher covalent character of the bonding for the former group. However, even though structural parameters and electronic factors can account for the latter effects,[43c] they cannot usually permit differentiation of actinide(III) and lanthanide(III) systems in terms of their relative stabilities, especially in the CN/NC coordination mode preference as experimentally noted. In fact, as noted by Arratia-Pérez et al.,[40] controversy already exists about the preference for the coordination of cyanide and isocyanide ligands toward the uranyl ion. These authors concluded that cyanide complexes might be more stable than their isocyanide congeners, although the energy difference is only 3.3 kcal mol^{-1}.

Energy Decomposition Analysis. In order to investigate the energetic factors driving the preferred coordination of the cyanide or isocyanide ligands to the uranium or cerium atoms,

dx.doi.org/10.1021/ic500939t | Inorg. Chem. 2014, 53, 6995−7013

respectively, in the complexes $[MN^*_3X_2]^{2-}$ (M = Ce or U, X = NC or CN), the coordination energies of these groups have been calculated following the reaction scheme:

$$MN^*_3 + 2X^- \rightarrow [MN^*_3X_2]^{2-} (X = CN \text{ or } NC)$$

The total bonding energies of the fragments (TBE_{frag}) computed at the spin unrestricted ZORA/BP86/TZP level (see Computational Details) are given in Table 9. The results are in agreement with experimental findings. Indeed, it can be seen, considering the actual structures, that the TBE_{frag} for the $Ce(NC)_2$ complex is higher (in absolute value) than the $Ce(CN)_2$ one, i.e., −127 versus −120.0 kcal mol^{-1}, whereas the opposite is obtained for the uranium complex, for which the most stable species is the $U(CN)_2$ one. The relative stability given by ΔE (kcal mol^{-1}) clearly highlights the difference in metal−ligand coordination between the Ce^{III} and U^{III} ions. Considering the different energy terms (Table 9), it is worth noting the following: (a) As expected, the E_{steric} term is more destabilizing for the uranium than for the cerium species due to the smaller metal−ligand distances in the former. (b) The steric term, which is summed from the Pauli repulsion (repulsion between electron pairs) and the stabilizing electrostatic interactions, reveals that the isocyanide binding mode is less sterically favorable than the cyanide binding mode. This is due to a higher Pauli repulsion consequent on shorter M−N bond lengths than M−C ones, whereas the electrostatic term does not vary significantly. (c) The orbital term E_{orb} (stabilizing energy due to orbital mixing) is greater in the $U(CN)_2$ than in the $U(NC)_2$ case, whereas the contrary is observed for the cerium species. This is due to the best energy matching between the 6d/5f orbitals and the upper cyano σ-donating MO with dominant C-character (see Figure 13) in the U^{III} systems. As shown by the MO analysis (Figure 14), the isocyanide M−NC interaction seems to be weaker than the cyanide M−CN one, as confirmed by metallic percentages which are more important in the latter. This could explain the energetic stability difference between the cyanide and isocyanide systems and the difference in preferred coordination modes to the uranium(III) and cerium(III) centers.

CONCLUSION

Reactions of the cerium(III) and uranium(III) complexes $[MN^*_3]$ (M = Ce, U; N* = $N(SiMe_3)_2$) and NR_4CN (R = Me, Et, or ^{n}Bu) or KCN in the presence of 18-crown-6 led to the successive formation of the cyanido-bridged dinuclear compounds $[M'][(MN^*_3)_2(\mu\text{-}CN)]$ and the mononuclear mono-, bis- and tris(cyanide) complexes $[M'][MN^*_3(CN)]$, $[M']_2[MN^*_3(CN)_2]$, and $[M']_2[MN^*_2(CN)_3]$ [M′ = NR_4 or K(18-crown-6); M = Ce and U]. The synthesis of these rare examples of mononuclear cyanide complexes of trivalent lanthanides and actinides, which would be interesting building blocks for the design of clusters and coordination polymers, confirms the remarkable coordinating capacity of the CN group in f element chemistry. Of special interest is the behavior of the bis(cyanide) complexes which were found to be in equilibrium with the mono(cyanide) complexes in solution and were slowly transformed into an equimolar mixture of the mono- and tris(cyanide) derivatives with elimination of a N* ligand. Crystals of the bis(cyanide) uranium complexes $[K(18\text{-crown-}6)]_2[UN^*_3(CN)_2]$ and its benzene solvate are isomorphous with those of the cerium counterparts, but they are not isostructural since the data revealed distinct coordination modes of the CN group, through the C or N atom to the U or Ce metal center, respectively. The preferential coordination of the cyanide and isocyanide ligands toward uranium or cerium in the $[MN^*_3(CN)_2]^{2-}$ complexes is well-corroborated by the consideration of the binding energies of these ligands to the metal ions and by the confrontation of the DFT optimized geometries and the structural crystal data. The electronic structure analysis showed that the stronger σ-donating ability of the cyanide ligand toward actinide systems over cerium counterparts in relation with the better energy matching between 6d/5f metal and ligand orbitals plays a significant role in the metal−ligand coordination preference. The effects of the cyanide and isocyanide coordination on the structural properties of the complexes, in particular the vibrational frequencies, have been rationalized considering electronic indices like bond orders. Remarkably, the distinct coordination of the cyanide ligand to the MN^*_3 complexes (M = Ce, U) cannot be considered as a general feature in Ln^{III}/An^{III} differentiation, since the M−C bonding mode of the CN ion was unambiguously determined in the bis(pentamethylcyclopentadienyl) compounds $[N^nBu_4]_2[M(Cp^*)_2(CN)_3]$ (M = Ce, U).[13] It seems likely that, in the bis(Cp*) series, the higher electron richness of the metal centers due to the presence of the electron donating Cp* ligands favors the coordination of the CN group through the C atom to both the Ce^{III} and U^{III} ions. Further studies including theoretical analysis are necessary to specify the influence of the nature of the metal and ancillary ligands, and the electron density around the metal, on the coordination mode of the cyanide ligand.

EXPERIMENTAL SECTION

General Procedure. All reactions were carried out under argon with the rigorous exclusion of air and water (<5 ppm oxygen or water) using standard Schlenk-vessel and vacuum line techniques or in a glovebox. Solvents were thoroughly dried by standard methods and distilled immediately before use. KCN (98%, Fluka), NEt_4CN (94%, Aldrich), N^nBu_4CN (95%, Aldrich), and $[NMe_4][BF_4]$ (Merck) have been used as received. NMe_4CN was prepared by salt metathesis between $[NMe_4][BF_4]$ and NEt_4CN in acetonitrile. $[CeN^*_3]$[44] and $[UN^*_3]$[45b] were prepared according to literature procedures. IR samples were prepared as Nujol mulls between KBr round cell windows and the spectra recorded on a PerkinElmer FT-IR 1725X spectrometer. The ^1H and $^{13}C\{^1H\}$ NMR spectra were recorded on a 200 or 500 MHz instrument at 20 °C when not otherwise specified and referenced internally using the residual protio solvent resonances relative to tetramethylsilane (δ 0). The signals corresponding to the CN ligands were not visible on the $^{13}C\{^1H\}$ NMR spectra. Elemental analyses were performed by Analytische Laboratorien at Lindlar (Germany) or by Medac Ltd. at Chobham (Surrey, U.K.). Note that, for each compound, elemental analyses were repeated several times with independently prepared batches and all gave similar results. The ^1H NMR spectra are free of impurities, so we attribute the low C, H, or N content to the fact that this is a cyanide and silicon rich molecule which prevents complete combustion, as noted previously.[46]

Synthesis of $[NEt_4][CeN^*_3(CN)]$ ($1a^{Et}$). A 50 mL flask was charged with $[CeN^*_3]$ (500 mg, 0.80 mmol) and NEt_4CN (125 mg, 0.76 mmol), and toluene (20 mL) was distilled in it under reduced pressure at −78 °C. After stirring for 6 h at 20 °C, the color of the solution turned from yellow to yellowish. The solution was filtered and evaporated to dryness, leaving a yellowish powder of $\mathbf{1a^{Et}}$ which was washed twice with pentane (25 mL), and dried under vacuum (590 mg, 99% with respect to NEt_4CN). Anal. Calcd for $C_{27}H_{74}N_5Si_6Ce$: C, 41.71; H, 9.59; N, 9.01. Found: C, 41.34; H, 9.27; N, 8.98. ^1H NMR (THF-d_8): δ_H 1.22 (s, 8H, NCH_2CH_3), −0.34 (s, 12H, NCH_2CH_3), −0.66 (s, 54H, $SiCH_3$). Decoalescence of the $SiCH_3$ signal was observed at −85 °C, but the slow-limit spectrum could not be attained.

dx.doi.org/10.1021/ic500939t | Inorg. Chem. 2014, 53, 6995−7013

^{1}H NMR (benzene-d_6): δ_H −0.26 (s, 54H, SiCH_3), −0.79 (s, 8H, NCH_2CH$_3$), −1.77 (s, 12H, NCH$_2$CH_3). ^{13}C{^{1}H} NMR (THF-d_8): δ 50.7 (s, NCH$_2$CH$_3$), 5.74 (s, NCH$_2$CH$_3$), 4.57 (s, SiCH$_3$). ^{13}C{^{1}H} NMR (benzene-d_6): δ_C 49.3 (s, NCH$_2$CH$_3$), 4.80 (s, SiCH$_3$), 4.77 (s, NCH$_2$CH$_3$). IR (Nujol): ν(CN) = 2063(s) cm^{-1}. Yellowish crystals obtained by diffusion of pentane into a concentrated solution of **1a^{Et}** in toluene, or by cooling a diethyl ether solution of **1a^{Et}** at −35 °C, were not suitable for X-ray diffraction studies.

Synthesis of [NEt$_4$][UN*$_3$(CN)] (1b^{Et}). A 50 mL flask was charged with [UN*$_3$] (500 mg, 0.70 mmol) and NEt$_4$CN (110 mg, 0.67 mmol), and THF (20 mL) was distilled in it under reduced pressure at −78 °C. The suspension was stirred for 8 h at 20 °C, and the color of the solution turned from dark purple to dark blue. After filtration, the volume of the solution was reduced to 2 mL, and pentane (40 mL) was added, leading to the precipitation of the dark blue powder of **1b^{Et}** which was washed twice with a 1:10 mixture of THF and pentane (20 mL) and dried under vacuum (450 mg, 78% with respect to NEt$_4$CN). Anal. Calcd for $C_{27}H_{74}N_5Si_6U$: C, 37.04; H, 8.52; N, 8.00. Found: C, 36.71; H, 8.34; N, 8.30. ^{1}H NMR (THF-d_8): δ_H 0.45 (m, 8H, NCH_2CH$_3$), −0.94 (m, 12H, NCH$_2$CH_3), −5.71 (s, 54H, SiCH_3). Decoalescence of the SiCH$_3$ signal was observed at −60 °C. ^{1}H NMR (THF-d_8, −90 °C): δ_H 4.9 (br, $w_{1/2}$ = 395 Hz, 27H, SiCH_3), −3.19 (s, 8H, NCH_2CH$_3$), −3.70 (s, 12H, NCH$_2$CH_3), −25.9 (br, $w_{1/2}$ = 395 Hz, 27H, SiCH_3). ^{1}H NMR (benzene-d_6): δ_H −2.83 (s, 8H, NCH_2CH$_3$), −3.41 (s, 12H, NCH$_2$CH_3), −5.28 (s, 54H, SiCH_3). ^{13}C{^{1}H} NMR (THF-d_8): δ_C 50.1 (s, NCH$_2$CH$_3$), 5.0 (s, NCH$_2$CH$_3$), −115.0 and −116.0 (s, SiCH$_3$). ^{13}C{^{1}H} NMR (benzene-d_6): δ_C 46.7(s, NCH$_2$CH$_3$), 2.2 (s, NCH$_2$CH$_3$), −109.0 and −111.0 (s, SiCH$_3$). IR (Nujol): ν(CN) = 2057 cm^{-1}. Dark blue crystals obtained by diffusion of pentane into a concentrated solution of **1b^{Et}** in toluene, or by cooling a diethyl ether solution of **1b^{Et}** at −35 °C, were not suitable for X-ray diffraction studies.

Crystals of [NMe$_4$][MN*$_3$(CN)] (M = Ce, 1a^{Me}; M = U, 1b^{Me}). (a) Colorless crystals of **1a^{Me}** were obtained by slowly cooling a solution of [CeN*$_3$] (10 mg, 16.1 μmol) and NMe$_4$CN (1.61 mg, 16.1 μmol) in a 1:5 mixture of toluene and pentane (1 mL) which was previously heated at 90 °C for 1 h. (b) Dark blue crystals of **1b^{Me}** were obtained either by cooling at −35 °C a solution of [UN*$_3$] (10 mg, 13.98 μmol) and NMe$_4$CN (1.4 mg, 13.98 μmol) in a 1:5 mixture of pentane and Et$_2$O (1 mL) which was first stirred for 2h at 20 °C, or by slow diffusion of pentane into a solution of [UN*$_3$] (10 mg, 13.98 μmol) and NMe$_4$CN (1.40 mg, 13.98 μmol) in THF (2 mL).

Reactions of [CeN*$_3$] and KCN. Crystals of [K(18-crown-6)][CeN*$_3$(CN)]·toluene (1′a·toluene) and [K(18-crown-6)-(THF)$_2$][(CeN*$_3$)$_2$(μ-CN)] (2′a). (a) An NMR tube was charged with [CeN*$_3$] (10.0 mg, 0.016 mmol) and KCN (5.2 mg, 0.080 mmol) in THF-d_8 (0.7 mL). After 30 min at 20 °C, the spectrum of the yellowish solution exhibited a signal at δ_H −2.60 attributed to the SiCH$_3$ groups of [K(THF)$_x$][(CeN*$_3$)$_2$(μ-CN)], and after 20 h, a second signal was visible at δ_H −0.74, corresponding to the SiCH$_3$ groups of [K(THF)$_x$][CeN*$_3$(CN)]. (b) An NMR tube was charged with [CeN*$_3$] (10.0 mg, 0.016 mmol), KCN (3.1 mg, 0.048 mmol), and 18-crown-6 (4.2 mg, 0.016 mmol) in toluene (1 mL), and the tube was sonicated for 1 h. After 12 h at −35 °C, bright yellow crystals of **1′a**·toluene were deposited. (c) Slow diffusion of pentane into a solution of [CeN*$_3$] (20.0 mg, 0.032 mmol), KCN (2.1 mg, 0.032 mmol), and 18-crown-6 (4.2 mg, 0.032 mmol) in THF (0.7 mL) led, after 7 days at 20 °C, to the formation of yellow crystals of **2′a**.

Reactions of [UN*$_3$] and KCN. Crystals of [K(18-crown-6)][UN*$_3$(CN)]·toluene (1′b·toluene) and [K(18-crown-6)]-[(UN*$_3$)$_2$(μ-CN)] (2′b). (a) An NMR tube was charged with [UN*$_3$] (10.0 mg, 0.014 mmol) and KCN (4.6 mg, 0.07 mmol) in THF-d_8 (0.7 mL). After 30 min at 20 °C, the spectrum of the dark purple solution exhibited two signals of equal intensities at δ_H −9.40 and −9.93 attributed to the SiCH$_3$ groups of [K(THF)$_x$][(UN*$_3$)$_2$(μ-CN)], the formation of which was complete after 5 h. After 20 h, the color of the solution has turned from dark purple to dark blue and the signal corresponding to the SiCH$_3$ groups of [K(THF)$_x$][UN*$_3$(CN)] was visible at δ_H −5.44. (b) An NMR tube was charged with [UN*$_3$] (17.0 mg, 0.023 mmol), KCN (4.2 mg, 0.07 mmol), and 18-crown-6 (6.3 mg, 0.023 mmol) in toluene (1 mL). After 2 days at −35 °C, dark blue crystals of **1′b**·toluene were deposited. (c) Slow diffusion of pentane into a solution of [UN*$_3$] (10.0 mg, 0.014 mmol), KCN (4.6 mg, 0.070 mmol), and 18-crown-6 (4.2 mg, 0.014 mmol) in toluene (0.7 mL) led, after 7 days at 20 °C, to the formation of dark blue crystals of **2′b**.

Synthesis of [NEt$_4$][(CeN*$_3$)$_2$(μ-CN)] (2a). (a) A 50 mL flask was charged with [CeN*$_3$] (206 mg, 0.33 mmol) and NEt$_4$CN (27.2 mg, 0.17 mmol), and THF (15 mL) was distilled in it under reduced pressure at −78 °C. After stirring for 15 h at 20 °C, the color of the solution turned from yellow to green-yellow. The solution was filtered and its volume reduced to 1 mL. Addition of pentane (25 mL) led to the precipitation of a pale yellow powder of **2a** which was filtered off, washed with pentane (25 mL), and dried under vacuum (175 mg, 40%). Anal. Calcd for $C_{45}H_{128}Ce_2N_8Si_{12}$: C, 38.64; H, 9.22; N, 8.01. Found: C, 38.00; H, 8.75; N, 7.3. ^{1}H NMR (THF-d_8): δ_H 3.19 (q, J = 7.0 Hz, 8H, NCH_2CH$_3$), 1.22 (t, J = 7.0 Hz, 12H, NCH$_2$CH_3), −2.60 (s, $w_{1/2}$ = 46 Hz, 108H, SiCH_3). The SiCH$_3$ signal at δ_H −2.60 was separated at −20 °C into two peaks of equal intensities at δ_H −3.27 and −3.38; broadening of these peaks was observed at lower temperatures, but the slow-limit spectrum was not attained. ^{1}H NMR (benzene-d_6): δ_H 1.82 (s, 8H, NCH_2CH$_3$), 0.49 (s, 12H, NCH$_2$CH_3), −2.11 (s, $w_{1/2}$ = 105 Hz,108H, SiCH_3). Compound **2a** is poorly soluble in benzene-d_6 at 20 °C. ^{13}C{^{1}H} NMR (THF-d_8): δ_C 52.8 (s, NCH$_2$CH$_3$), 7.3 (s, NCH$_2$CH$_3$), 3.9 (s, SiCH$_3$). ^{13}C{^{1}H} NMR (benzene-d_6): δ_C 51.7 (s, NCH$_2$CH$_3$), 6.7 (s, NCH$_2$CH$_3$), 4.0 (s, SiCH$_3$). IR (Nujol): ν(CN) = 2108(s) cm^{-1}. (b) A 100 mL flask was charged with [CeN*$_3$] (262 mg, 0.42 mmol) and **1a** (320 mg, 0.41 mmol), and toluene (20 mL) was distilled in it under reduced pressure at −78 °C. After stirring for 6 h at 20 °C, the color of the solution turned from yellow to yellowish and the yellow powder of **2a** was deposited. Addition of pentane (5 mL) led to the complete precipitation of **2a**, which was filtered off, washed with a 5:1 mixture of toluene and pentane (5 mL), and dried under vacuum. A yellowish microcrystalline powder of **2a** was obtained after crystallization from toluene (328 mg, 55%).

Synthesis of [NEt$_4$][(UN*$_3$)$_2$(μ-CN)] (2b). (a) A 50 mL flask was charged with [UN*$_3$] (250 mg, 0.35 mmol) and NEt$_4$CN (28.8 mg, 0.175 mmol), and toluene (25 mL) was distilled in it under reduced pressure at −78 °C. After stirring for 2 days at 20 °C, the color of the solution turned from dark purple to dark blue. The solution was evaporated to dryness, and the resulting blue solid was extracted with diethyl ether (30 mL). The volume of the solution was reduced to 2 mL, and addition of pentane (30 mL) led to the precipitation of a dark blue powder of **2b** which was filtered off, washed again with pentane (25 mL), and dried under vacuum (240 mg, 86%). Anal. Calcd for $C_{45}H_{128}U_2N_8Si_{12}$: C, 33.89; H, 8.09; N, 7.03. Found: C, 33.67; H, 7.91; N, 6.55. ^{1}H NMR (THF-d_8): δ_H 3.75 (s, 8H, NCH_2CH$_3$), 1.46 (s, 12H, NCH$_2$CH_3), −9.54 and −10.07 (s, 2 × 54H, SiCH_3). ^{1}H NMR (benzene-d_6, 40 °C): δ_H 0.09 (s, 8H, NCH_2CH$_3$), −1.12 (s, 12H, NCH$_2$CH_3), −8.20 and −8.68 (s, 2 × 54H, SiCH_3). Compound **2b** is poorly soluble in benzene-d_6 at 20 °C. ^{13}C{^{1}H} NMR (THF-d_8): δ_C 52.6 (s, NCH$_2$CH$_3$), 7.1 (s, NCH$_2$CH$_3$), −101.8, −102.5, −104.7, and −105.6 (s, SiCH$_3$). IR (Nujol): ν(CN) = 2096(s) cm^{-1}. (b) A 50 mL flask was charged with [UN*$_3$] (100 mg, 0.14 mmol) in toluene (15 mL), and a solution of **1b^{Et}** (119 mg, 0.14 mmol) in toluene (15 mL) was added dropwise. After stirring for 36 h at 20 °C, the volume of the dark blue suspension was reduced to 3 mL, and addition of pentane (25 mL) led to the precipitation of the dark blue powder of **2b**, which was filtered off, washed three times with pentane (25 mL), and dried under vacuum (175 mg, 79%). Dark blue crystals obtained by slowly cooling down from 100 to 20 °C a concentrated solution of **2b** in toluene were not suitable for X-ray diffraction studies.

Reactions of 1a^{Et} and [UN*$_3$], 1b^{Et} and [CeN*$_3$], 2a and 2b, or [UN*$_3$] and [CeN*$_3$] and NEt$_4$CN. An NMR tube was charged either with (a) **1a^{Et}** (12.4 mg, 15.9 μmol) and [UN*$_3$] (11.4 mg, 15.9 μmol), or (b) **1b^{Et}** (8.5 mg, 9.8 μmol) and [CeN*$_3$] (6.1 mg, 9.8 μmol), or (c) **2a** (4.4 mg, 3.1 μmol) and **2b** (5.0 mg, 3.1 μmol), or (d) [CeN*$_3$] (10.0 mg, 16.1 μmol) and [UN*$_3$] (11.5 mg, 16.1 μmol) and NEt$_4$CN (2.7 mg, 16.1 μmol) in THF-d_8 (0.7 mL). After 1 h at 20 °C, the

dx.doi.org/10.1021/ic500939t | Inorg. Chem. 2014, 53, 6995−7013

spectra of the blue solutions were identical, showing the signals of **2a** and **2b** and new signals attributed to $[NEt_4][(CeN^*_3)(\mu\text{-}CN/NC)(UN^*_3)]$. ^{1}H NMR (500 MHz, THF-d_8, −5 °C): δ_H 4.12 (s, 8H, NCH_2CH_3), 1.92 (s, 12H, NCH_2CH_3), −2.84 and −2.96 (two equal singlets, 27H, N^*_3 of **2a**), −6.11 and −6.25 (two singlets of relative intensity 1:4, 27H, $N^*_3Ce-CN-UN^*_3$ and $N^*_3Ce-NC-UN^*_3$), −7.17 and −7.71 (two singlets of relative intensity 4:1, 27H, $N^*_3Ce-NC-UN^*_3$ and $N^*_3Ce-CN-UN^*_3$), −10.33 and −10.87 (two equal singlets, 27H, N^*_3 of **2b**). Irradiation of the $SiMe_3$ signals of **2a** caused a decrease in the intensity of the N^*_3Ce signals of $[NEt_4][(CeN^*_3)(\mu\text{-}CN/NC)(UN^*_3)]$.

Synthesis of $[N^nBu_4]_2[CeN^*_3(CN)_2]$ (3a). A 50 mL flask was charged with $[CeN^*_3]$ (200 mg, 0.32 mmol) and N^nBu_4CN (198 mg, 0.68 mmol) in THF (10 mL). The yellow solution turned immediately colorless. After stirring for 5 min at 20 °C, the solution was filtered and evaporated to dryness, leaving an off-white solid which was extracted in Et_2O (25 mL). After evaporation of the solvent, the off-white powder of **3a** was dried under vacuum (152 mg, 41% with respect to $[CeN^*_3]$). Anal. Calcd for $C_{52}H_{126}CeN_7Si_6$: C, 53.92; H, 10.97; N, 8.47. Found: C, 53.69; H, 11.19; N, 8.74. ^{1}H NMR (THF-d_8): δ_H 2.74 (m, 16H, $NCH_2CH_2CH_2CH_3$), 1.17 (m, 16H, $NCH_2CH_2CH_2CH_3$), 1.03 (m, 16H, $NCH_2CH_2CH_2CH_3$), 0.73 (m, 24H, $NCH_2CH_2CH_2CH_3$), −0.50 (s, 54H, $SiCH_3$). ^{1}H NMR (benzene-d_6): δ_H 1.49 (m, 16H, $NCH_2CH_2CH_2CH_3$), 0.75 (m, 16H, $NCH_2CH_2CH_2CH_3$), 0.44 (m, 24H, $NCH_2CH_2CH_2CH_3$), 0.15 (m, 16H, $NCH_2CH_2CH_2CH_3$), −0.06 (s, 54H, $SiCH_3$). $^{13}C\{^1H\}$ NMR (THF-d_8): δ_C 58.7 (s, $NCH_2CH_2CH_2CH_3$), 24.3 (s, $NCH_2CH_2CH_2CH_3$), 20.2 (s, $NCH_2CH_2CH_2CH_3$), 13.8 (s, $NCH_2CH_2CH_2CH_3$), 4.4 (s, $SiCH_3$). $^{13}C\{^1H\}$ NMR (benzene-d_6): δ_C 57.3 (s, $NCH_2CH_2CH_2CH_3$), 23.0 (s, $NCH_2CH_2CH_2CH_3$), 19.1 (s, $NCH_2CH_2CH_2CH_3$), 13.4 (s, $NCH_2CH_2CH_2CH_3$), 4.8 (s, $SiCH_3$). IR (Nujol): ν(CN) = 2074 (s), 2173 (m) cm^{-1}. Pale yellow crystals of **3a** were obtained by crystallization from a mixture of THF and Et_2O.

Synthesis of $[N^nBu_4]_2[UN^*_3(CN)_2]$ (3b). A 50 mL flask was charged with $[UN^*_3]$ (200 mg, 0.28 mmol) and N^nBu_4CN (164 mg, 0.56 mmol), and THF (10 mL) was distilled in it under reduced pressure at −78 °C. After stirring for 2 h at 20 °C, the color of the solution turned from dark purple to dark blue. The solution was filtered and its volume reduced to 2 mL. Addition of pentane led to the precipitation of a turquoise blue powder which was filtered off and dissolved in toluene (5 mL). The oily product obtained upon addition of pentane (25 mL) was triturated and transformed into a turquoise blue powder of **3b** which was filtered off and dried under vacuum (196 mg, 55%). Anal. Calcd for $C_{52}H_{126}N_7Si_6U$: C, 49.72; H, 10.11; N, 7.81. Found: C, 49.64; H, 10.66; N, 7.80. ^{1}H NMR (THF-d_8): δ_H 2.45 (m, 16H, $NCH_2CH_2CH_2CH_3$), 1.75 (m, 32H, $NCH_2CH_2CH_2CH_3$), 1.15 (m, 24H, $NCH_2CH_2CH_2CH_3$), −4.5 (br, $w_{1/2}$ = 180 Hz, 54H, $SiCH_3$). ^{1}H NMR (benzene-d_6): δ_H 0.74 (s, 16H, $NCH_2CH_2CH_2CH_3$), 0.17 (s, 40H, $NCH_2CH_2CH_2CH_3$), −0.44 (s, 16H, $NCH_2CH_2CH_2CH_3$), −4.9 (br, $w_{1/2}$ = 80 Hz, 54H, $SiCH_3$). $^{13}C\{^1H\}$ NMR (THF-d_8): δ_C 56.8 (s, $NCH_2CH_2CH_2CH_3$), 23.1 (s, $NCH_2CH_2CH_2CH_3$), 19.0 (s, $NCH_2CH_2CH_2CH_3$), 13.1 (s, $NCH_2CH_2CH_2CH_3$), −96.2 (s, $SiCH_3$). IR (Nujol): ν(CN) = 2058 (s), 2197 (m) cm^{-1}. Dark blue crystals obtained by slow diffusion of pentane into a concentrated solution of **3b** in toluene were not suitable for X-ray diffraction studies.

Synthesis of $[K(18\text{-crown-}6)]_2[CeN^*_3(CN)_2]$ (3′a). A 50 mL flask was charged with $[CeN^*_3]$ (200 mg, 0.32 mmol), KCN (62.9 mg, 0.96 mmol), and 18-crown-6 (170 mg, 0.64 mmol), and THF (15 mL) was distilled in it under reduced pressure at −78 °C. The color of the solution turned immediately from yellow to pale yellow, and after stirring for 15 h at 20 °C, the solution was cooled at 0 °C and filtered and the remaining solid extracted in cold THF (15 mL). The volume of the THF solution was then reduced to 2 mL, and addition of pentane (25 mL) led to the precipitation of an off-white powder of **3′a** which was filtered off. The mono(cyanide) **1′a** was eliminated by extraction in a 1:10 mixture of THF and pentane (20 mL), and the off-white powder of **3′a** was dried under vacuum (140 mg, 34%). Anal. Calcd for $C_{44}H_{102}CeK_2N_5O_{12}Si_6$: C, 41.28; H, 8.03; N, 5.47. Found: C, 38.32; H, 7.65; N, 5.20. ^{1}H NMR (THF-d_8): δ_H 3.14 (s, 48H, 18-crown-6), −0.56 (s, 54H, $SiCH_3$). ^{1}H NMR (benzene-d_6): δ_H 2.21 (s, 48H, 18-crown-6), −0.08 (s, 54H, $SiCH_3$). $^{13}C\{^1H\}$ NMR (THF-d_8): δ 70.8 (s, 18-crown-6), 4.6 (s, $SiCH_3$). $^{13}C\{^1H\}$ NMR (benzene-d_6): δ_C 69.2 (s, 48H, 18-crown-6), 4.7 (s, $SiCH_3$). IR (Nujol): ν(CN) = 2078 (s), 2171 (m) cm^{-1}. Slow diffusion of pentane into a solution of $[CeN^*_3]$ (10.0 mg, 0.016 mmol), KCN (5.24 mg, 0.08 mmol), and 18-crown-6 (12.7 mg, 0.048 mmol) in THF (1 mL) led to the formation, after 6 days at 20 °C, of yellow crystals of **3′a** (blue under incident light). Bluish crystals of **3′a**·2benzene were obtained by crystallization of **3′a** from benzene.

Synthesis of $[K(18\text{-crown-}6)]_2[UN^*_3(CN)_2]$ (3′b). A 50 mL flask was charged with $[UN^*_3]$ (200 mg, 0.28 mmol), KCN (54.6 mg, 0.84 mmol), and 18-crown-6 (147.7 mg, 0.56 mmol), and THF (20 mL) was distilled in it under reduced pressure at −78 °C. After stirring for 15 h at 20 °C, the color of the solution turned from dark purple to dark blue. The solution was filtered, and its volume was reduced to 5 mL. Addition of hexane (25 mL) led to the precipitation of the turquoise blue powder of **3′b** which was filtered off, washed with a 1:5 mixture of THF and hexane (25 mL), and dried under vacuum (126.7 mg, 33%). Anal. Calcd for $C_{44}H_{102}K_2N_5O_{12}Si_6U$: C, 38.35; H, 7.46; N, 5.08. Found: C, 33.95; H, 6.44; N, 5.61. ^{1}H NMR (THF-d_8): δ_H 2.73 (s, 48H, 18-crown-6), −5.63 (br, $w_{1/2}$ = 200 Hz, 54H, $SiCH_3$). ^{1}H NMR (THF-d_8, 10 °C): δ_H 2.86 (s, 48H, 18-crown-6), −3.75 (br, $w_{1/2}$ = 180 Hz, 27H, $SiCH_3$ of **3′b**), −5.90 (br, $w_{1/2}$ = 150 Hz, 27H, $SiCH_3$ of **1′b**). ^{1}H NMR (THF-d_8, 0 °C): δ_H 2.90 (s, 48H, 18-crown-6), −3.86 (br, $w_{1/2}$ = 107 Hz, 39H, $SiCH_3$ of **3′b**), −6.26 (br, $w_{1/2}$ = 175 Hz, 15H, $SiCH_3$ of **1′b**). ^{1}H NMR (toluene-d_8): δ_H 1.51 (s, 48H, 18-crown-6), −2.54 (br, $w_{1/2}$ = 160 Hz, 22H, $SiCH_3$ of **3′b**), −4.99 (br, $w_{1/2}$ = 140 Hz, 32H, $SiCH_3$ of **1′b**). $^{13}C\{^1H\}$ NMR (THF-d_8): δ_C 69.8 (s, 18-crown-6), −113.5 (br s, $SiCH_3$). The **3′b**/**1′b** ratio increased upon lowering the temperature and/or addition of KCN. IR (Nujol): ν(CN) = 2063 (s), 2091 (m) cm^{-1}. Slow diffusion of pentane into a solution of $[UN^*_3]$ (10.0 mg, 0.014 mmol), KCN (4.55 mg, 0.07 mmol), and 18-crown-6 (7.38 mg, 0.028 mmol) in THF (1 mL) led to the formation, after 6 days at 20 °C, of dark blue crystals of **3′b**. Crystals of **3′b** were also obtained by crystallization from THF, while dark blue crystals of **3′b**·2benzene were obtained by crystallization of **3′b** from benzene.

Synthesis of $[N^nBu_4]_2[CeN^*_2(CN)_3]$ (4a). (a) An NMR tube was charged with **3a** (10 mg) in THF-d_8 (0.7 mL). After 15 h at 20 °C, the spectrum showed that **3a** was completely transformed into an equimolar mixture of $\mathbf{1a^{Bu}}$ (δ $SiMe_3$ −0.68), **4a** (δ $SiMe_3$ −4.10), and $[N^nBu_4]N^*$ (δ_H 0). (b) A 50 mL flask was charged with $[CeN^*_3]$ (200 mg, 0.32 mmol) and N^nBu_4CN (1.95 eq., 183 mg, 0.63 mmol), and THF (15 mL) was condensed in it under vacuum at −78 °C. After stirring for 15 h at 20 °C, the pale yellow solution was filtered and its volume reduced to 2 mL. Addition of Et_2O (20 mL) led to the precipitation of an off-white powder which was filtered off. The mono(cyanide) $\mathbf{1a^{Bu}}$ was eliminated by extraction in a 1:10 mixture of THF and Et_2O (20 mL), and the off-white powder of **4a** was dried under vacuum (134 mg, 41%). Anal. Calcd for $C_{47}H_{108}CeN_7Si_4$: C, 55.13; H, 10.63; N, 9.58. Found: C, 53.83; H, 9.84; N, 9.76. ^{1}H NMR (THF-d_8): δ_H 2.74 (m, 16H, $NCH_2CH_2CH_2CH_3$), 1.89 (m, 16H, $NCH_2CH_2CH_2CH_3$), 1.31 (m, 40H, $NCH_2CH_2CH_2CH_3$), −4.10 (s, $w_{1/2}$ = 40 Hz, 36H, $SiCH_3$). $^{13}C\{^1H\}$ NMR (THF-d_8): δ_C 58.7 (s, $NCH_2CH_2CH_2CH_3$), 24.6 (s, $NCH_2CH_2CH_2CH_3$), 20.9 (s, $NCH_2CH_2CH_2CH_3$), 14.5 (s, $NCH_2CH_2CH_2CH_3$), 0.7 (s, $SiCH_3$). Compound **4a** is poorly soluble in benzene-d_6 preventing ^{1}H and ^{13}C NMR characterization. IR (Nujol): ν(CN) = 2065 (s), 2175 (m) cm^{-1}. Crystals of **4a** were obtained by crystallization from THF. (c) A 50 mL flask was charged with $[CeN^*_3]$ (200 mg, 0.32 mmol) and N^nBu_4CN (283 mg, 0.96 mmol), and THF (30 mL) was condensed in it under vacuum at −78 °C. After stirring for 20 h at 20 °C, the pale yellow solution was filtered and its volume reduced to 2 mL. Addition of Et_2O (25 mL) led to the precipitation of an off-white powder of **4a** which was filtered off, washed with Et_2O (15 mL) and toluene (2 × 15 mL), and dried under vacuum (207 mg, 63%).

Synthesis of $[N^nBu_4]_2[UN^*_2(CN)_3]$ (4b). (a) An NMR tube was charged with **3b** (10 mg) in THF-d_8 (0.7 mL). After 3 days at 20 °C, the spectrum showed that **3b** was completely transformed into an equimolar mixture of $\mathbf{1b^{Bu}}$ (δ_H $SiMe_3$ −5.68), **4b** (δ_H $SiMe_3$ −6.81),

dx.doi.org/10.1021/ic500939t | Inorg. Chem. 2014, 53, 6995−7013

and [N^{n}Bu$_4$]N* (δ_H 0). (b) A 50 mL flask was charged with [UN*$_3$] (300 mg, 0.42 mmol) and N^{n}Bu$_4$CN (246 mg, 0.84 mmol), and THF (15 mL) was condensed in it under vacuum at −78 °C. After stirring for 4 days at 20 °C, the black solution was filtered and its volume reduced to 2 mL. Addition of Et$_2$O (25 mL) led to the precipitation of a black powder which was filtered off. The mono(cyanide) **1b** was eliminated by extraction in Et$_2$O until a colorless washing solution was obtained, and the black powder of **4b** was dried under vacuum (174 mg, 37%). Anal. Calcd for $C_{47}H_{108}N_7Si_4U$: C, 50.32; H, 9.70; N, 8.74. Found: C, 46.38; H, 8.99; N, 8.34. ^{1}H NMR (THF-d_8): δ_H 1.05 (m, 16H, NCH$_2$CH$_2$CH$_2$CH$_3$), 0.92 (m, 24H, NCH$_2$CH$_2$CH$_2$CH$_3$), 0.41 (m, 16H, NCH$_2$CH$_2$CH$_2$CH$_3$), −0.31 (m, 16H, NCH$_2$CH$_2$CH$_2$CH$_3$), −6.81 (s, 36H, SiCH$_3$). ^{13}C{^{1}H} NMR (THF-d_8): δ_C 54.7 (s, NCH$_2$CH$_2$CH$_2$CH$_3$), 22.1 (s, NCH$_2$CH$_2$CH$_2$CH$_3$), 18.3 (s, NCH$_2$CH$_2$CH$_2$CH$_3$), 12.9 (s, NCH$_2$CH$_2$CH$_2$CH$_3$), −95.9 (s, SiCH$_3$). Compound **4b** is poorly soluble in benzene-d_6 preventing ^{1}H and ^{13}C NMR characterization. IR (Nujol): ν(CN) = 2059 (s), 2089 (m), 2179 (m) cm^{-1}. Blue-black crystals of **4b** were obtained by crystallization from a 1:1 mixture of Et$_2$O and THF. (c) A 50 mL flask was charged with [UN*$_3$] (335 mg, 0.42 mmol) and N^{n}Bu$_4$CN (3 equiv , 411 mg, 1.47 mmol), and THF (30 mL) was condensed in it under vacuum at −78 °C. After stirring for 4 days at 20 °C, the black solution was filtered and its volume reduced to 2 mL. Addition of Et$_2$O (25 mL) led to the precipitation of a black powder of **4b** which was filtered off, washed with Et$_2$O (15 mL) and toluene (2 × 15 mL), and dried under vacuum (307 mg, 59%).

Crystallography. The data were collected at 150(2) K on a Nonius Kappa-CCD area detector diffractometer[47] using graphite-monochromated Mo Kα radiation (λ = 0.710 73 Å). The crystals were introduced into glass capillaries with a protecting coating of Paratone-N oil (Hampton Research). The unit cell parameters were determined from 10 frames, then refined on all data. The data (combinations of φ- and ω-scans with a minimum redundancy of at least 4 for 90% of the reflections) were processed with HKL2000.[48] Absorption effects were corrected empirically with the program SCALEPACK.[48] The structures were solved by direct methods or Patterson map interpretation (except when an isomorphous model was available), expanded by subsequent Fourier-difference synthesis, and refined by full-matrix least-squares on F^2 with SHELXL-97.[49] All non-hydrogen atoms were refined with anisotropic displacement parameters. In most structures in which the cyanide anion is not necessarily disordered around a symmetry element (as is the case in **2′a** and **2′b**), it has been possible to determine unambiguously the location of the carbon and nitrogen atoms by selecting the solution giving the most satisfying refined displacement parameters (i.e., close to one another for a bridging cyanide, or giving the most regular progression from metal to terminal atom in the case of monodentate cyanides). However, this assignment is doubtful in **1a^{Me}**, **1b^{Me}**, **1′b**·toluene and **4a**; in **1′b**·toluene, the best solution was found when assuming C/N disorder (see below). The hydrogen atoms were introduced at calculated positions and were treated as riding atoms with an isotropic displacement parameter equal to 1.2 times that of the parent atom (1.5 for CH$_3$). Special details are as follows.

1a^{Me}. With the location of the carbon and nitrogen atoms in the two cyanide groups being ambiguous, refinement of a disordered model was attempted, with each position occupied by refined fractions of carbon and nitrogen atoms, constrained to retain the same positional and displacement parameters. This refinement led to the predominance (by more than 80%) of different bonding modes in the two independent molecules. Although the refined values of these fractions may not be very reliable, they are indicative of the best solution in each case, corresponding to Ce(1)−N(1)−C(1) and Ce(2)−C(20)−N(5), and these bonding modes have been retained for the final refinement. Restraints on displacement parameters had to be applied for some carbon atoms in the methyl groups.

1b^{Me}. The carbon and nitrogen atoms of the two cyanide ions have been located at the position giving the most satisfying progression of the displacement parameters in the three-atoms sequence, giving U−C−N as the most likely arrangement, but the reverse position or a mixture of both cannot be ruled out. Restraints on displacement parameters had to be applied for some carbon atoms in the methyl groups.

1′a·toluene. The C−N bond length had to be restrained since it refined freely to a value lower than 1 Å, with the result that although the assignment of the C and N atoms based on displacement parameters is rather clear, it cannot be considered as unambiguous.

1′b·toluene. None of the two possible orientations of the cyanide ion is satisfactory, both leading to Hirshfeld test anomalies. This ion was thus modeled as being disordered, with each position occupied by refined fractions of carbon and nitrogen atoms, constrained to retain the same positional and displacement parameters, which gives about 66% uranium bonding by nitrogen.

2′a and **2′b**. The cyanide ion is disordered around a symmetry element, and it has been modeled with a 50:50 mixture of carbon and nitrogen at each site.

3a. One of the N^{n}Bu$_4$ counterions is badly disordered, and most of its carbon atoms have been refined over two positions with occupancy parameters of 0.5. Only one terminal carbon atom is disordered in the other counterion. Restraints for several bond lengths and displacement parameters had to be applied for the atoms in the disordered parts.

3′a·2benzene and **3′b**·2benzene. The benzene ring was refined as an idealized hexagon.

4a·0.5THF. The unit cell is metrically close to tetragonal or orthorhombic (indeed, the complex **4b**·Et$_2$O crystallizes in the orthorhombic system with unit cell parameters very close to those in **4a**·0.5THF), but the R_{int} factor in the orthorhombic system is about twice as large as in the monoclinic system, and although ADDSYM (PLATON[50]) suggests $P2_12_12_1$ as a possible space group with 86% fit, no correct solution could be found in this space group. The structure was thus refined in $P2_1$, as corresponding to a pseudomerohedral twin with the 2-fold rotation axis [101] as twin element. With this space group being chiral, refinement of the other components resulting from further inversion twinning was attempted, but this gave corresponding BASF parameters close to 0 and only the main twin component was thus considered (BASF 0.71). In addition to twinning, the crystal was of very low quality and weakly diffracting, and many restraints on bond lengths, angles and displacement parameters had to be applied for the four N^{n}Bu$_4$ counterions and the THF solvent molecule. One terminal carbon atom of a N^{n}Bu$_4$ cation is disordered over two positions which were refined with occupancy parameters constrained to unity. The carbon and nitrogen atoms in the cyanide ions cannot be clearly differentiated on the basis of the displacement parameters. The solution which was deemed best was chosen, but the reverse choice cannot be ruled out. Some voids in the lattice likely indicate the presence of other, unresolved solvent molecules, but with the residual electron density in the voids being quite small, the use of SQUEEZE[50] did not improve the results.

Crystal data and structure refinement parameters are given in Table 10. The molecular plots were drawn with ORTEP-3.[51]

Computational Details. All molecular geometries of cyanide [MN*$_3$(CN)$_2$]$^{2-}$ and isocyanide [MN*$_3$(NC)$_2$]$^{2-}$ (M^{+3} = Ce, U ; N* = N(SiMe$_3$)$_2$) complexes were fully optimized, starting from crystal structures when available, at relativistic DFT level of theory using the Amsterdam Density Functional (ADF2013.01) program package.[52c] Scalar relativistic effects were taken into account via the Zeroth Order Regular Approximation (ZORA).[52e−g] The Vosko−Wilk−Nusair functional (VWN)[53a] for the Local Density Approximation (LDA) and gradient corrections for exchange and correlation of Becke and Perdew,[53b,c] respectively, i.e., the BP86 functional, have been used, particularly for the geometry optimizations and the analytical computation of the frequencies of the normal modes of vibration. Several theoretical studies have shown that such a ZORA/BP86/TZP approach reproduces the experimental geometries and ground state properties of f-element compounds with a satisfying accuracy.[39] Triple-ζ Slater-type valence orbitals (STO) augmented by one set of polarization functions were used for all atoms. For all elements, the basis sets were taken from the ADF/ZORA/TZP database. The 1s core electrons were frozen, respectively, for carbon C[1s], nitrogen N[1s], and Si[2p]. The Ln[4d] and An[5d] valence space of the heavy elements includes the 4f/5s/5p/5d/6s/6p and 5f/6s/6p/6d/7s/7p

dx.doi.org/10.1021/ic500939t | Inorg. Chem. 2014, 53, 6995−7013

Table 10. Crystal Data and Structure Refinement Details

	1a^{Me}	**1b^{Me}**	**1′a**·toluene	**1′b**·toluene	**2′a**	**2′b**	**3a**
chemical formula	$C_{23}H_{66}CeN_5Si_6$	$C_{23}H_{66}N_5Si_6U$	$C_{76}H_{172}Ce_2K_2N_8O_{12}Si_{12}$	$C_{76}H_{172}K_2N_8O_{12}Si_{12}U_2$	$C_{57}H_{148}Ce_2KN_7O_8Si_{12}$	$C_{49}H_{132}KN_7O_6Si_{12}U_2$	$C_{52}H_{126}CeN_7Si_6$
M (g mol^{-1})	721.47	819.38	2085.74	2281.56	1716.24	1767.86	1158.26
cryst syst	orthorhombic	orthorhombic	monoclinic	monoclinic	monoclinic	triclinic	orthorhombic
space group	$Pna2_1$	$Pna2_1$	$P2_1/n$	$P2_1/n$	$C2/c$	$P\bar{1}$	$Pbca$
a (Å)	18.8938(6)	18.8915(6)	15.2749(5)	15.2713(4)	34.250(2)	12.0596(5)	19.4222(13)
b (Å)	23.1641(12)	23.1576(13)	21.3372(5)	21.3931(7)	17.7252(14)	13.2544(5)	19.5146(14)
c (Å)	18.6838(10)	18.6384(11)	17.6492(6)	17.6644(5)	15.8540(11)	15.2109(3)	37.947(3)
α (deg)	90	90	90	90	90	108.812(2)	90
β (deg)	90	90	99.897(2)	99.916(2)	103.845(4)	103.255(2)	90
γ (deg)	90	90	90	90	90	104.341(2)	90
V (Å^3)	8177.1(7)	8154.0(7)	5666.7(3)	5684.8(3)	9345.1(11)	2099.24(14)	14382.5(18)
Z	8	8	2	2	4	1	8
D_{calcd} (g cm^{-3})	1.172	1.335	1.222	1.333	1.220	1.398	1.070
μ(Mo Kα) (mm^{-1})	1.307	4.176	1.043	3.094	1.203	4.113	0.766
F(000)	3048	3320	2204	2340	3624	894	5032
reflns collcd	170 276	174 718	177 756	409 421	139 149	127 475	341 949
indep reflns	15 059	15 016	17 282	17 334	12 016	12 821	13 624
obsd reflns [$I > 2\sigma(I)$]	11 155	10 847	11 000	12 191	6498	10 838	7047
R_{int}	0.058	0.064	0.043	0.033	0.080	0.043	0.065
params refined	674	674	524	525	412	366	733
R1	0.054	0.054	0.039	0.031	0.044	0.025	0.075
wR2	0.096	0.077	0.090	0.074	0.081	0.053	0.238
S	1.055	1.041	0.985	0.986	0.910	0.992	1.057
$\Delta\rho_{min}$ (e Å^{-3})	−0.66	−1.15	−0.93	−0.55	−0.64	−0.92	−0.90
$\Delta\rho_{max}$ (e Å^{-3})	0.51	0.94	0.89	1.00	0.42	0.65	1.67

	3′a	**3′b**	**3′a**·2benzene	**3′b**·2benzene	**4a**·0.5THF	**4b**·Et_2O
chemical formula	$C_{44}H_{102}CeK_2N_5O_{12}Si_6$	$C_{44}H_{102}K_2N_5O_{12}Si_6U$	$C_{56}H_{114}CeK_2N_5O_{12}Si_6$	$C_{56}H_{114}K_2N_5O_{12}Si_6U$	$C_{49}H_{112}CeN_7O_{0.5}Si_4$	$C_{51}H_{118}N_7OSi_4U$
M (g mol^{-1})	1280.17	1378.08	1436.38	1534.29	1059.94	1195.91
cryst syst	monoclinic	monoclinic	orthorhombic	orthorhombic	monoclinic	orthorhombic
space group	$P2_1/c$	$P2_1/c$	$Pbcn$	$Pbcn$	$P2_1$	$P2_12_12_1$
a (Å)	12.7847(8)	12.7839(9)	16.0382(7)	16.0629(3)	13.6516(11)	13.3981(3)
b (Å)	38.9616(13)	38.907(3)	19.8665(8)	19.8765(6)	35.807(2)	13.6398(6)
c (Å)	13.8920(8)	13.9099(5)	24.6850(6)	24.6155(8)	13.7407(12)	36.6421(15)
α (deg)	90	90	90	90	90	90
β (deg)	103.759(3)	103.920(4)	90	90	90.064(5)	90
γ (deg)	90	90	90	90	90	90
V (Å^3)	6721.2(6)	6715.4(8)	7865.2(5)	7859.1(4)	6716.8(9)	6696.3(4)
Z	4	4	4	4	4	4
D_{calcd} (g cm^{-3})	1.265	1.363	1.213	1.297	1.048	1.186
μ(Mo Kα) (mm^{-1})	0.959	2.699	0.827	2.314	0.782	2.531
F(000)	2708	2844	3044	3180	2292	2516
reflns collcd	162 141	91 984	170 967	173 731	77 439	116 698
indep reflns	20 495	12 703	11 997	11 980	22 180	12 705

dx.doi.org/10.1021/ic500939t | Inorg. Chem. 2014, 53, 6995−7013

Table 10. continued

	3′a	3′b	3′a·2benzene	3′b·2benzene	4a·0.5THF	4b·Et_2O
obsd refins [$I > 2\sigma(I)$]	12 233	7421	7520	7216	12 248	10 672
R_{int}	0.093	0.092	0.039	0.036	0.094	0.032
params refined	649	649	368	368	1154	600
R1	0.044	0.051	0.039	0.032	0.075	0.054
wR2	0.093	0.095	0.099	0.075	0.185	0.157
S	0.910	0.940	1.019	0.982	0.956	1.024
$\Delta\rho_{min}$ (e Å^{-3})	−1.73	−0.99	−0.41	−0.77	−1.19	−1.02
$\Delta\rho_{max}$ (e Å^{-3})	0.81	1.43	0.45	0.49	1.05	3.53

shells, respectively (small core approximation). Finally, for all complexes, we considered the highest ($2S + 1$) spin state as the ground state configuration, i.e., doublet (f^1) spin states for the Ce^{III} and quartet (f^3) for U^{III} systems. In addition, in order to reinforce the reliability of our results, computations have also been carried out using the Perdew–Wang (PW91)[53e] and Perdew–Burke–Ernzerhof (PBE)[53f] functionals.

In order to provide a better understanding of the metal–ligand bonding, a Natural Population Analysis (NPA)[41a] and a Quantum Theory Atom-in-Molecules (QTAIM)[41b] analysis have been carried out. NPA and QTAIM topological approaches have been shown to lead to reliable results for f-element complexes.[41d−g] Among QTAIM descriptors are the points of lowest electron density between each atom pair, i.e., bond critical points (BCP) for which electron density ρ_c and its energy density H_c can be defined (the subscript indicates the electron density at the BCP). As was established in previous works,[41d−f] bonding interactions may be characterized according to these characteristic data (ρ_c and H_c). Indeed, the values of $\rho_c >$ ca. 0.2 e/bohr^3 are typical of covalent (shared shell) interactions, and those of $\rho_c <$ ca. 0.1 e/bohr^3 indicate more ionic interactions (closed shell interactions). Energy density H_c is negative for bonding interactions (covalent electrons), in relation with the concentration of electron density along the bond path linking the bonded atoms.

As the ADF program supplies an energetic decomposition of the metal–ligand bonding into chemically useful terms, we have carried out spin-unrestricted fragment calculations considering the two molecular moieties in interaction, i.e., MN^*_3 and X_2 (X = CN/NC) for the $[MN^*_3X_2]^{2-}$ complexes (M = Ce or U). We remind the reader that this energetic decomposition, which is based on the transition-state method developed by Morokuma, and then by Ziegler et al.,[42a−c] provides insights into the balance of the different bonding electronic or electrostatic factors at work between the isolated cation or metallic moiety and the ligands in a complex.

Thus, within this scheme, the resulting total bonding energy TBE_{frag} between two fragments can be decomposed into two terms as $TBE_{frag} = E_{steric} + E_{orb}$, where the E_{steric} term is, in our case, the steric interaction energy between the MN^*_3 metallic fragment and the CN or NC ligand and E_{orb} is the orbital (covalent) contribution to the metal–CN/NC bond. The steric energy term (E_{steric}) is itself decomposed into a destabilizing term E_{Pauli}, the electronic repulsion due to the Pauli principle, and E_{ES}, the stabilizing electrostatic energy between the two fragments $E_{steric} = E_{Pauli} + E_{ES}$. The bonding energies have been computed at the ZORA/BP86/TZP level.

■ ASSOCIATED CONTENT

Ⓢ Supporting Information

Tables of crystal data, atomic positions and displacement parameters, anisotropic displacement parameters, and bond lengths and bond angles in CIF format. NMR spectra, equilibrium data, as well as DFT optimized geometries. This material is available free of charge via the Internet at http://pubs.acs.org.

■ AUTHOR INFORMATION

Corresponding Authors

*E-mail: jean-claude.berthet@cea.fr.
*E-mail: abdou.boucekkine@univ-rennes1.fr.
*E-mail: michel.ephritikhine@cea.fr.

Notes

The authors declare no competing financial interest.

■ ACKNOWLEDGMENTS

Dr. G. Nocton (Ecole Polytechnique, Palaiseau) is thanked for crystal testing on an Apex X-ray diffractometer. The authors are grateful to GENCI-IDRIS and GENCI-CINES for an allocation of computing time (Grant 2013-080649).

REFERENCES

(1) McColm, I. J.; Thompson, S. J. *J. Inorg. Nucl. Chem.* **1972**, *34*, 3801.
(2) Bagnall, K. W.; Baptista, J. L. *J. Inorg. Nucl. Chem.* **1970**, *32*, 2283.
(3) Kanellakopulos, B.; Dornberger, E.; Billich, H. *J. Organomet. Chem.* **1974**, *76*, C42.
(4) Kalsotra, B. L.; Multani, R. K.; Jain, B. D. *J. Inorg. Nucl. Chem.* **1972**, *34*, 2265.
(5) Bagnall, K. W.; Plews, M. J.; Brown, D.; Fischer, R. D.; Klähne, E.; Landgraf, G. W.; Sienel, G. R. *J. Chem. Soc., Dalton Trans.* **1982**, 1999.
(6) Adam, R.; Villiers, C.; Ephritikhine, M.; Lance, M.; Nierlich, M.; Vigner, J. *J. Organomet. Chem.* **1993**, *445*, 99.
(7) Mehdoui, T. Thèse de Doctorat, Université Paris XI, 2005.
(8) Maynadié, J.; Berthet, J. C.; Thuéry, P.; Ephritikhine, M. *Organometallics* **2007**, *26*, 4585.
(9) Evans, W. J.; Drummond, D. K. *Organometallics* **1988**, *7*, 797.
(10) Obora, Y.; Ohta, T.; Stern, C. L.; Marks, T. J. *J. Am. Chem. Soc.* **1997**, *119*, 3745.
(11) Evans, W. J.; Forrestal, K. J.; Ziller, J. W. *J. Am. Chem. Soc.* **1998**, *120*, 9273.
(12) Evans, W. J.; Mueller, T. J.; Ziller, J. W. *Chem.—Eur. J.* **2010**, *16*, 964.
(13) Maynadié, J.; Berthet, J. C.; Thuéry, P.; Ephritikhine, M. *Organometallics* **2007**, *26*, 2623.
(14) Evans, W. J.; Montalvo, E.; Foster, S. E.; Harada, K. A.; Ziller, J. W. *Organometallics* **2007**, *26*, 2904.
(15) Tanase, S.; Reedijk, J. *Coord. Chem. Rev.* **2006**, *250*, 2501.
(16) del Mar Conejo, M.; Parry, J. S.; Carmona, E.; Schultz, M.; Brennann, J. G.; Beshouri, S. M.; Andersen, R. A.; Rogers, R. D.; Coles, S.; Hursthouse, M. *Chem.—Eur. J.* **1999**, *5*, 3000.
(17) Zi, G.; Jia, L.; Werkema, E. L.; Walter, M. D.; Gottfriedsen, J. P.; Andersen, R. A. *Organometallics* **2005**, *24*, 4251.
(18) Ren, W.; Zi, G.; Fang, D. C.; Walter, M. D. *J. Am. Chem. Soc.* **2011**, *133*, 13183.
(19) Maynadié, J.; Barros, N.; Berthet, J. C.; Thuéry, P.; Maron, L.; Ephritikhine, M. *Angew. Chem., Int. Ed.* **2007**, *46*, 2010.
(20) Berthet, J. C.; Thuéry, P.; Ephritikhine, M. *Organometallics* **2008**, *27*, 1664.
(21) (a) Hervé, A.; Garin, N.; Thuéry, P.; Ephritikhine, M.; Berthet, J. C. *Chem. Commun.* **2013**, *49*, 6304. (b) Hervé, A.; Thuéry, P.; Ephritikhine, M.; Berthet, J. C. *Organometallics* **2014**, *33*, 2088.
(22) Bénaud, O.; Berthet, J. C.; Thuéry, P.; Ephritikhine, M. *Inorg. Chem.* **2011**, *50*, 12204.
(23) Straka, M.; Patzschke, M.; Pyykkö, P. *Theor. Chem. Acc.* **2003**, *109*, 332.
(24) Clavaguéra-Sarrio, C.; Hoyau, S.; Ismail, N.; Marsden, C. J. *J. Phys. Chem. A* **2003**, *107*, 4515.
(25) Sonnenberg, J. L.; Hay, P. J.; Martin, R. L.; Bursten, B. E. *Inorg. Chem.* **2005**, *44*, 2255.
(26) Berthet, J. C.; Thuéry, P.; Ephritikhine, M. *Chem. Commun.* **2007**, 604.
(27) Maynadié, J.; Berthet, J. C.; Thuéry, P.; Ephritikhine, M. *Chem. Commun.* **2007**, 486.
(28) Fortier, S.; Brown, J. L.; Kaltsoyannis, N.; Wu, G.; Hayton, T. W. *Inorg. Chem.* **2012**, *51*, 1625.
(29) Shannon, R. D. *Acta Crystallogr., Sect. A* **1976**, *32*, 751.
(30) (a) Brennan, J. G.; Stults, S. D.; Andersen, R. A.; Zalkin, A. *Organometallics* **1988**, *7*, 1329. (b) Rivière, C.; Nierlich, M.; Ephritikhine, M.; Madic, C. *Inorg. Chem.* **2001**, *40*, 4428. (c) Karmazin, L.; Mazzanti, M.; Pécaut, J. *Chem. Commun.* **2002**, 654. (d) Berthet, J. C.; Miquel, Y.; Iveson, P. B.; Nierlich, M.; Thuéry, P.; Madic, C.; Ephritikhine, M. *J. Chem. Soc., Dalton Trans.* **2002**, 3265. (e) Cendrowski-Guillaume, S. M.; Le Gland, G.; Nierlich, M.; Ephritikhine, M. *Eur. J. Inorg. Chem.* **2003**, 1388. (f) Villiers, C.; Thuéry, P.; Ephritikhine, M. *Eur. J. Inorg. Chem.* **2004**, 4624. (g) Mehdoui, T.; Berthet, J. C.; Thuéry, P.; Ephritikhine, M. *Dalton Trans.* **2004**, 579. (h) Mehdoui, T.; Berthet, J. C.; Thuéry, P.; Ephritikhine, M. *Chem. Commun.* **2005**, 2860. (i) Roger, M.; Belkhiri, L.; Thuéry, P.; Arliguie, T.; Fourmigué, M.; Boucekkine, A.; Ephritikhine, M. *Organometallics* **2005**, *24*, 4940. (j) Berthet, J. C.; Nierlich, M.; Miquel, Y.; Madic, C.; Ephritikhine, M. *Dalton Trans.* **2005**, 369. (k) Mehdoui, T.; Berthet, J. C.; Thuéry, P.; Salmon, L.; Rivière, E.; Ephritikhine, M. *Chem.—Eur. J.* **2005**, *11*, 6994. (l) Roger, M.; Barros, N.; Arliguie, T.; Thuéry, P.; Maron, L.; Ephritikhine, M. *J. Am. Chem. Soc.* **2006**, *128*, 8790. (m) Roger, M.; Belkhiri, L.; Arliguie, T.; Thuéry, P.; Boucekkine, A.; Ephritikhine, M. *Organometallics* **2008**, *27*, 33.
(31) (a) Lappert, M. F., Power, P. P., Sanger, A. R., Srivastava, R. C. In *Metal and Metalloid Amides: Syntheses, Structures and Physical and Chemical Properties*; Ellis Horwood/Wiley: New York, 1980. (b) Berthet, J. C.; Ephritikhine, M. *Coord. Chem. Rev.* **1998**, *178–180*, 83.
(32) (a) Forsen, S.; Hoffman, R. A. *J. Chem. Phys.* **1963**, *39*, 2892. (b) Mann, B. E. In *Comprehensive Organometallic Chemistry*; Wilkinson, G., Stone, F. G. A., Abel, E. W., Eds.; Pergamon Press: Oxford, U.K., 1982; Vol. *3*, Chapter 20, p 89.
(33) (a) McGeary, M. J.; Folting, K.; Streib, W. E.; Huffman, J. C.; Caulton, K. G. *Polyhedron* **1991**, *10*, 2699. (b) Yao, S.; Xiong, Y.; Vogt, M.; Grützmacher, H.; Herwig, C.; Limberg, C.; Driess, M. *Angew. Chem., Int. Ed.* **2009**, *48*, 8107. (c) Broomsgrove, A. E. J.; Addy, D. A.; Di Paolo, A.; Morgan, I. R.; Bresner, C.; Chislett, V.; Fallis, I. A.; Thompson, A. L.; Vidovic, D.; Aldridge, S. *Inorg. Chem.* **2010**, *49*, 157. (d) Ilyukhin, A.; Dobrokhotova, Z.; Petrosyants, S.; Novotortsev, V. *Polyhedron* **2011**, *30*, 2654.
(34) Figuerola, A.; Diaz, C.; Ribas, J.; Tangoulis, V.; Granell, J.; Lloret, F.; Mahía, J.; Maestro, M. *Inorg. Chem.* **2003**, *42*, 641.
(35) Johnson, S. E.; Knobler, C. B. *Organometallics* **1992**, *11*, 3684.
(36) (a) Hartwig, J. F. In *Organotransition Metal Chemistry, From Bonding to Catalysis*; University Science Books: Sausalito, CA, 2010; Chapter 3, p 103. (b) Hanusa, T. P.; Burkey, D. J. In *Encyclopedia of Inorganic Compounds*; King, R. B., Ed.; J. Wiley and Sons: Chichester, U.K., 1994; Vol. *2*, p 943. (c) Mock, M. T.; Kieber-Emmons, M. T.; Popescu, C. V.; Gasda, P.; Yap, G. P. A.; Riordan, C. G. *Inorg. Chim. Acta* **2009**, *362*, 4553.
(37) Fang, M.; Farnaby, J. H.; Ziller, J. W.; Bates, J. E.; Furche, F.; Evans, W. J. *J. Am. Chem. Soc.* **2012**, *134*, 6064.
(38) Deacon, G. B.; Delbridge, E. E.; Forsyth, C. M. *Angew. Chem., Int. Ed.* **1999**, *38*, 1766.
(39) (a) Roger, M.; Belkhiri, L.; Arliguie, T.; Thuéry, P.; Boucekkine, A.; Ephritikhine, M. *Organometallics* **2008**, *27*, 33. (b) Gaunt, A. J.; Reilly, S. D.; Enriquez, A. E.; Scott, B. L.; Ibers, J. A.; Sekar, P.; Ingram, K. I. M.; Kaltsoyannis, N.; Neu, M. P. *Inorg. Chem.* **2008**, *47*, 29. (c) Gaunt, A. J.; Reilly, S. D.; Enriquez, A. E.; Scott, B. J.; Ibers, J. A.; Sekar, P.; Ingram, K. I. M.; Kaltsoyannis, N.; Neu, M. P. *Inorg. Chem.* **2008**, *47*, 29. (d) Roger, M.; Belkhiri, L.; Thuéry, P.; Bouaoud, S. E.; Boucekkine, A.; Ephritikhine, M. *Inorg. Chem.* **2009**, *48*, 221. (e) Meskaldji, S.; Belkhiri, L.; Arliguie, T.; Fourmigué, M.; Ephritikhine, M.; Boucekkine, A. *Inorg. Chem.* **2010**, *49*, 3192. (f) Meskaldji, S.; Zaiter, A.; Belkhiri, L.; Boucekkine, A. *Theor. Chem. Acc.* **2012**, *131*, 1151.
(40) Páez-Hernández, D.; Ramírez-Tagle, R.; Codorniu-Hernández, E.; Montero-Cabrera, L. A.; Arratia-Pérez, R. *Polyhedron* **2010**, *29*, 975.
(41) (a) Reed, A. E.; Curtiss, L. A.; Weinhold, F. *Chem. Rev.* **1988**, *88*, 899. (b) Bader, R. F. W. *Atoms in Molecules: A Quantum Theory*; OUP: Oxford, 1990. (c) Mulliken, R. S. *J. Chem. Phys.* **1955**, *23*, 1833. (d) Mountain, A. R. E.; Kaltsoyannis, N. *Dalton Trans.* **2013**, *42*, 13477. (e) Jones, M. B.; Gaunt, A. J.; Gordon, J. C.; Kaltsoyannis, N.; Neu, M. P.; Scott, B. L. *Chem. Sci.* **2013**, *4*, 1189. (f) Schnaars, D. D.; Gaunt, A. J.; Hayton, T. W.; Jones, M. B.; Kirker, I.; Kaltsoyannis, N.; May, I.; Reilly, S. D.; Scott, B. L.; Wu, G. *Inorg. Chem.* **2012**, *51*, 8557. (g) Vlaisavljevich, B.; Miró, P.; Cramer, C. J.; Gagliardi, L.; Infante, I.; Liddle, S. T. *Chem.—Eur. J.* **2011**, *17*, 8424. (h) Arnold, P. L.; Turner, Z. R.; Kaltsoyannis, N.; Pelekanaki, P.; Bellabarba, R. M.; Tooze, R. P. *Chem.—Eur. J.* **2010**, *16*, 9623.
(42) (a) Morokuma, K. *J. Chem. Phys.* **1971**, *55*, 1236. (b) Kitaura, K.; Morokuma, K. *Int. J. Quantum Chem.* **1976**, *10*, 325. (c) Ziegler, T.;

Rauk, A. *Theor. Chim. Acta* **1977**, *46*, 1. (d) Mayer, I. *Chem. Phys. Lett.* **1983**, *7*, 270.
(43) (a) Nalewajski, R. F.; Mrozek, J. *Int. J. Quantum Chem.* **1994**, *51*, 187. (b) Nalewajski, R. F.; Mrozek, J.; Michalak, A. *Int. J. Quantum Chem.* **1997**, *6*, 589. (c) Neidig, M. L.; Clark, D. L.; Martin, R. L. *Coord. Chem. Rev.* **2013**, *257*, 394.
(44) Rees, W. S.; Oliver Just, O.; Van Derveer, D. S. *J. Mater. Chem.* **1999**, *99*, 249.
(45) (a) Andersen, R. A. *Inorg. Chem.* **1979**, *18*, 1507. (b) Monreal, M. J.; Thomson, R. K.; Cantat, T.; Travia, N. E.; Scott, B. L.; Kiplinger, J. L. *Organometallics* **2011**, *30*, 2031.
(46) (a) Levanda, C.; Streitwieser, A. *Inorg. Chem.* **1981**, *20*, 656. (b) Nishiura, M.; Hou, Z.; Wakatsuki, Y. *Organometallics* **2004**, *23*, 1359. (c) Hitchcock, P. B.; Lappert, M. F.; Maron, L.; Protchenko, A. V. *Angew. Chem., Int. Ed.* **2008**, *47*, 1488. (d) Berthet, J. C.; Thuéry, P.; Garin, N.; Dognon, J. P.; Cantat, T.; Ephritikhine, M. *J. Am. Chem. Soc.* **2013**, *135*, 10003. (e) King, D. M.; Tuna, F.; McMaster, J.; Lewis, W.; Blake, A. J.; McInnes, E. J. L.; Liddle, S. T. *Angew. Chem., Int. Ed.* **2013**, *52*, 4921.
(47) Hooft, R. W. W. *COLLECT*; Nonius BV: Delft, The Netherlands, 1998.
(48) Otwinowski, Z.; Minor, W. *Methods Enzymol.* **1997**, *276*, 307.
(49) Sheldrick, G. M. *Acta Crystallogr., Sect. A* **2008**, *64*, 112.
(50) Spek, A. L. *J. Appl. Crystallogr.* **2003**, *36*, 7.
(51) Farrugia, L. J. *J. Appl. Crystallogr.* **1997**, *30*, 565.
(52) (a) te Velde, G.; Bickelhaupt, F. M.; van Gisbergen, S. J. A.; Fonseca Guerra, C.; Baerends, E. J.; Snijders, J. G.; Ziegler, T. *J. Comput. Chem.* **2001**, *22*, 931. (b) Fonseca Guerra, C.; Snijders, J. G.; te Velde, G.; Baerends, E. J. *Theor. Chem. Acc.* **1998**, *99*, 391. (c) *ADF2013*; SCM, Theoretical Chemistry, Vrije Universiteit: Amsterdam, The Netherlands, http://www.scm.com. (d) Becke, A. D. *J. Chem. Phys.* **1988**, *88*, 2547. (e) van Lenthe, E.; Baerends, E. J.; Snijders, J. G. *J. Chem. Phys.* **1993**, *99*, 4597. (f) van Lenthe, E.; Baerends, E. J.; Snijders, J. G. *J. Chem. Phys.* **1994**, *101*, 9783. (g) van Lenthe, E.; Ehlers, A. E.; Baerends, E. J. *J. Chem. Phys.* **1999**, *110*, 8943.
(53) (a) Vosko, S. D.; Wilk, L.; Nusair, M. *Can. J. Chem.* **1990**, *58*, 1200. (b) Becke, A. D. *Phys. Rev. A* **1988**, *38*, 3098. (c) Perdew, J. P. *Phys. Rev. B* **1986**, *34*, 7406. (d) Perdew, J. P. In *Electronic Structure of Solids '91*;Ziesche, P., Eschrig, H., Eds.; Akademie Verlag: Berlin, 1991; p 11. (e) Perdew, J. P.; Wang, Y. *Phys. Rev. B* **1992**, *45*, 13244. (f) Perdew, J. P.; Burke, K.; Ernzerhof, M. *Phys. Rev. Lett.* **1996**, *77*, 3865. (g) Perdew, J. P.; Burke, K.; Ernzerhof, M. *Phys. Rev. Lett.* **1997**, *78*, 1396.

NOTE ADDED AFTER ASAP PUBLICATION

This paper originally posted ASAP on June 16, 2014 with an error in Table 10. The corrected version was reposted on June 18, 2014.